



# Upper tropospheric CH<sub>4</sub> and N<sub>2</sub>O retrievals from MetOp/IASI within the project MUSICA

Omaira E. García<sup>1</sup>, Eliezer Sepúlveda<sup>2,1</sup>, Matthias Schneider<sup>3</sup>, Andreas Wiegeler<sup>3</sup>, Christian Borger<sup>3</sup>, Frank Hase<sup>3</sup>, Sabine Barthlott<sup>3</sup>, Thomas Blumenstock<sup>3</sup>, and Angel M. de Frutos<sup>2</sup>

<sup>1</sup>Izaña Atmospheric Research Centre (IARC), Agencia Estatal de Meteorología (AEMET), Santa Cruz de Tenerife, Spain

<sup>2</sup>Atmospheric Optics Group (GOA), University of Valladolid, Valladolid, Spain

<sup>3</sup>Institute of Meteorology and Climate Research (IMK-ASF), Karlsruhe Institute of Technology (KIT), Karlsruhe, Germany

Correspondence to: O.E. García (ogarcia@amet.es)

**Abstract.** This paper presents upper tropospheric methane (CH<sub>4</sub>) and nitrous oxide (N<sub>2</sub>O) concentrations retrieved from thermal infrared spectra as observed by the remote sensor IASI (Infrared Atmospheric Sounding Interferometer) on-board the EU-METSAT/MetOp meteorological satellites. The CH<sub>4</sub> and N<sub>2</sub>O mixing ratios are retrieved as side products of the MetOp/IASI retrieval developed for the European Research Council project MUSICA (MUlti-platform remote Sensing of Isotopologues for investigating the Cycle of Atmospheric water). The MUSICA/IASI CH<sub>4</sub> and N<sub>2</sub>O retrieval strategy is described in detail as well as their characterisation in terms of the vertical resolution and expected errors. Theoretically, we document that MUSICA/IASI products can capture the upper tropospheric CH<sub>4</sub> and N<sub>2</sub>O variability (at ≈300-350 hPa) with a precision better than 2%. We compare the remote sensing data to coincident high precision aircraft vertical profiles taken within the HIPPER Pole-to-Pole Observations (HIPPO) project and empirically estimate a precision of 2.1% (38.2 ppbv) for each individual IASI CH<sub>4</sub> observation. The precision is improved to 1.7% (32.1 ppbv) for IASI data that have been averaged within 2°x2° boxes. For N<sub>2</sub>O the empirically estimated precision is 2.7% (8.7 ppbv) for each individual observation and 2.1% (6.9 ppbv) for the 2°x2° averages. The empirical study works with data from the missions HIPPO1 and HIPPO5, which cover latitudes between 67°S and 80°N during typical winter and summer conditions in both hemispheres, thus being reasonably representative for global observation during different seasons.

In addition, we present a product that combines the CH<sub>4</sub> and N<sub>2</sub>O retrieval estimates. The combination is made a-posteriori and we theoretically and empirically show that the combined product has a much better precision than the individual CH<sub>4</sub> and N<sub>2</sub>O products. For the combined product the theoretical precision is 0.8% and the comparison with HIPPO data gives an empirical precision estimate of 1.5% (26.3 ppbv) when considering all individual IASI observations and of 1.2% (21.8 ppbv) for the 2°x2° averages. In the case that the horizontal, vertical and temporal variation of N<sub>2</sub>O can be robustly modeled, we can easily reconstruct CH<sub>4</sub> from the combined product and generate high quality IASI CH<sub>4</sub> data.

## 1 Introduction

After carbon dioxide (CO<sub>2</sub>), CH<sub>4</sub> and N<sub>2</sub>O are currently the most important well-mixed greenhouse gases (GHGs). Although they are much less abundant than CO<sub>2</sub> in the atmosphere, their Global Warming Potentials are significantly larger: CH<sub>4</sub> and



$\text{N}_2\text{O}$  are about 35 and 300 times, respectively, more efficient than  $\text{CO}_2$  trapping outgoing long wave radiation, on a 100-yr time horizon (Stocker et al., 2013). It is well recognized that the imbalance between their sources and sinks has unquestionably increased during the last few centuries, but the exact location, intensity and nature of  $\text{CH}_4$  and  $\text{N}_2\text{O}$  sources and sinks are not as well understood as those for  $\text{CO}_2$  (Crevoisier et al., 2009). The knowledge of today's  $\text{CH}_4$  and  $\text{N}_2\text{O}$  sources/sinks, their spatial distribution and their variability in time is essential for understanding their role in the carbon and nitrogen cycles and for a reliable prediction of future atmospheric  $\text{CH}_4$  and  $\text{N}_2\text{O}$  abundances. The latter is important for predicting radiative forcing as well as ozone recovery (both  $\text{CH}_4$  and  $\text{N}_2\text{O}$  act as ozone depleting substances). Existing observations on fluxes of  $\text{CH}_4$  and  $\text{N}_2\text{O}$  from soils and oceans are still insufficient to adequately address these crucial tasks (e.g. Huang et al., 2008; Kort et al., 2011).

Since the late 1970s, surface in-situ measurements of these GHGs are systematically taken within the GAW programme (Global Atmospheric Watch-World Meteorological Organisation, [www.wmo.int](http://www.wmo.int)). These observations have proved to be very precise and, thus, are indispensable inputs for inverse methods and chemical transport models (e.g. Bousquet et al., 2011; Cressot et al., 2014). More recently, ground-based remote sensing FTS (Fourier Transform Infrared Spectrometer) experiments also routinely provided high-quality  $\text{CH}_4$  and  $\text{N}_2\text{O}$  concentrations in the framework of the international networks NDACC (Network for the Detection of Atmospheric Composition Change, [www.adc.ucar.edu/irwg](http://www.adc.ucar.edu/irwg), Schneider et al., 2005; Angelbratt et al., 2011; Sepúlveda et al., 2014) and TCCON (Total Carbon Column Observing Network, [www.tccon.caltech.edu](http://www.tccon.caltech.edu), Wunch et al., 2011). However, both surface in-situ and ground-based remote sensing measurements sample only a small fraction of the whole atmosphere. In this context, space-based remote sensing instruments have an outstanding importance due to their global coverage, allowing a comprehensive monitoring of the GHGs sources/sinks and their global distributions as well as a more complete understanding of the atmospheric processes affecting their flux variations.

The great potential of the space-based instruments to observe global  $\text{CH}_4$  and  $\text{N}_2\text{O}$  distributions has extensively been reported in literature. Examples of these satellite measurements by using different spectral ranges and observing geometries are those from ENVISAT/MIPAS (Michelson Interferometer for Passive Atmospheric Sounding, Payan et al., 2009; Plieninger et al., 2015), ENVISAT/SCIAMACHY (SCanning Imaging Absorption SpectroMeter for Atmospheric CHartography, Frankenberg et al., 2006), SCISAT-1/ACE (Atmospheric Chemistry Experiment, De Mazière et al., 2008), AURA/TES (Tropospheric Emission Spectrometer, Wecht et al., 2012; Worden et al., 2012) or GOSAT/TANSO-FTS (Thermal And Near infrared Sensor for carbon Observation, Yokota et al., 2009). Although the thermal nadir instruments have limited sensitivity to the  $\text{CH}_4$  and  $\text{N}_2\text{O}$  concentration variations in the lower troposphere due to the lack of thermal contrast, they have the clear advantage of observing under a large variety of conditions (day and night, over land and ocean, and for partly cloudy scenes), increasing significantly their global coverage (Clerbaux et al., 2009; Wecht et al., 2012). Among the current thermal nadir sensors, IASI (Infrared Atmospheric Sounding Interferometer, Blumstein et al., 2004) has special relevance, because it successfully combines the meteorology requirements for weather forecasting (high spatial coverage and a relatively good temporal resolution) and the atmospheric chemistry needs (high spectral resolution thereby allowing for trace gas retrievals), with a long-term data availability. Its mission is guaranteed until 2022 through the meteorological satellites MetOp, the space component of the EUMETSAT (European Organisation for the Exploitation of Meteorological Satellites, [www.eumetsat.int](http://www.eumetsat.int)) Polar



System (EPS) programme: the first sensor (IASI-A) was launched in October 2006 on-board MetOp-A, the second (IASI-B) was launched in September 2012 on-board MetOp-B and the third (IASI-C) is expected to be launched in October 2018 aboard MetOp-C. As a result of its well-recognized great performance, the IASI mission will be starting in the 2020s with IASI-NG (IASI New Generation, Crevoisier et al., 2014). IASI-NG has a further improved spectral resolution and radiometric performance and will flown on three successive MetOp-Second Generation (SG) satellites of the EPS-SG system, giving a perspective of data records until the late 2030s. All this is very promising for monitoring atmospheric composition in the long term, and IASI and IASI-NG are key instruments for EUMETSAT's contribution to Copernicus, the European system for monitoring the Earth (e.g. Clerbaux et al., 2009; Crevoisier et al., 2009; August et al., 2012).

The MUSICA/IASI retrieval focuses on tropospheric water vapour isotopologues (Schneider and Hase, 2011; Wiegeler et al., 2014; Schneider et al., 2016), but also provides upper tropospheric CH<sub>4</sub> and N<sub>2</sub>O as side products. The presentation of the MUSICA/IASI CH<sub>4</sub> and N<sub>2</sub>O products as well as their empirical validation using the HIPPO Pole-to-Pole Observations (HIPPO) database are the main goals of this paper. In addition, we will use the HIPPO data to empirically validate EUMETSAT's operational Level 2 (L2) IASI CH<sub>4</sub> and N<sub>2</sub>O products and briefly discuss their quality in comparison to the quality of the MUSICA products.

The paper is structured as follows: Section 2 presents the MUSICA/IASI CH<sub>4</sub> and N<sub>2</sub>O products (retrieval strategy and theoretical characterisation in terms of vertical sensitivity and error estimation). Section 3 discusses the possibility of combining the CH<sub>4</sub> retrieval data with the co-retrieved N<sub>2</sub>O product and demonstrates that the combined product has theoretically a significantly higher precision than the individual CH<sub>4</sub> and N<sub>2</sub>O products. Section 4 addresses the empirical validation of the MUSICA/IASI products, detailing the validation dataset and the comparison strategy used as well as the inter-comparison results. Section 5 presents the spatial and temporal coverage of the MUSICA/IASI products and very briefly discusses the observed latitudinal gradients and seasonal cycles. Section 6 shows a consistency assessment between the MUSICA/IASI products from the two IASI sensors currently in orbit (MetOp-A/IASI and MetOp-B/IASI). Section 7 briefly extends the validation exercise showing respective results for the EUMETSAT operational L2 IASI CH<sub>4</sub> and N<sub>2</sub>O products. Section 8 summarizes the main results and conclusions of this work.

## 25 2 MUSICA/IASI CH<sub>4</sub> and N<sub>2</sub>O products

### 2.1 MetOp/IASI sensor

The IASI sensor is a nadir-viewing Fourier Transform spectrometer developed by CNES (Centre National d'Etudes Spatiales, www.cnes.fr) in cooperation with EUMETSAT. It is on-board the EUMETSAT MetOp satellites, which operate in a polar and low Earth orbit since 2006. With 14 orbits per day in a sun-synchronous orbit (09:30 and 21:30 Local Solar Time equator crossing) IASI can provide global observations twice per day. IASI measures thermal infrared radiation emitted by the Earth's surface and the atmosphere between 645–2760 cm<sup>-1</sup> with an apodized spectral resolution of 0.5 cm<sup>-1</sup> and scans the surface perpendicular to the satellite's flight track with 30 individual views, covering a surface swath width of about 2200 km. Each individual view consists of 4 individual ground pixels (IFOV) of about 12 km diameter at nadir. The calibrated IASI radiances



for these 120 field of views are disseminated by EUMETSAT as Level 1C (L1C), together with additional information about observation geometry.

## 2.2 CH<sub>4</sub> and N<sub>2</sub>O retrieval strategy

MUSICA MetOp/IASI retrieval focuses on the optimal estimation of tropospheric water vapour concentrations and on the ratio between the isotopologues HDO and H<sub>2</sub>O (Schneider and Hase, 2011; Wiegele et al., 2014; Schneider et al., 2015). The retrieval analyses the thermal emission spectra recorded by IASI in the 1190-1400 cm<sup>-1</sup> spectral region and uses the thermal nadir retrieval algorithm PROFFIT-nadir (Schneider and Hase, 2011; Wiegele et al., 2014). In the analysed spectral region CH<sub>4</sub> and N<sub>2</sub>O have important spectroscopic signatures and are retrieved simultaneously to the water vapour isotopologues. The PROFFIT-nadir retrieval code has been developed in support of the project MUSICA for analysing thermal nadir spectra. It is an extension of the PROFFIT code used since many years for analysing high resolution solar absorption infrared spectra (PROFile Fit, Hase et al., 2004).

The CH<sub>4</sub> and N<sub>2</sub>O VMR (Volume Mixing Ratio) profiles are derived, on a logarithmic scale, using an ad-hoc Tikhonov-Philips slope constraint (TP1 constraint, Tikhonov, 1963) with a strong regularisation. This is almost equivalent to a scaling retrieval and only allows for very small changes in the shape of the a-priori profile. The CH<sub>4</sub> and N<sub>2</sub>O retrievals are made simultaneously to retrievals of the water vapour isotopologues as well as to retrievals of the minor interfering species CO<sub>2</sub> and HNO<sub>3</sub>. While the minor interferences of CO<sub>2</sub> and HNO<sub>3</sub> can be well accounted for by scaling the a-priori CO<sub>2</sub> and HNO<sub>3</sub> profiles (scaling retrieval), the interferences of the water vapour isotopologues are very strong and the application of a sophisticated retrieval method is needed. The MUSICA retrieval performs an optimal estimation of isotopologues on a logarithmic scale (Schneider and Hase, 2011; Wiegele et al., 2014).

A high quality water vapour isotopologue retrieval is crucial for obtaining a CH<sub>4</sub> and N<sub>2</sub>O product with a reasonable quality. This is illustrated in Fig. 1, which shows an example of the radiance measured by IASI and simulated by PROFFIT-nadir in the spectral region used for the CH<sub>4</sub> and N<sub>2</sub>O retrievals as well as the change in IASI radiances due to a change of CH<sub>4</sub> by +5%, of N<sub>2</sub>O by +2%, and of H<sub>2</sub>O by +100%, whereby 5%, 2% and 100% are typical values for the respective trace gas variations (please note the different y-axis scale for H<sub>2</sub>O spectral signatures). As observed, the spectral signatures of H<sub>2</sub>O variations are very strong if compared to the signatures of CH<sub>4</sub> and N<sub>2</sub>O variations, meaning that the quality of the CH<sub>4</sub> and N<sub>2</sub>O products depends on a correct interpretation of the spectroscopic interferences of the water vapour isotopologues.

For all the fitted species we use the same a-priori profiles for all retrievals, i.e. they do not vary on a daily, seasonal or latitudinal basis. Thereby, all the observed atmospheric variations are induced by the IASI observations rather than the a-priori information. The a-priori profiles of the different species are typical low-latitudes profiles taken from WACCM (Whole Atmosphere Community Climate Model-version 5, <http://waccm.acd.ucar.edu>) provided by NCAR (National Center for Atmospheric Research, J. Hannigan, private communication). They are climatologies provided at a spatial resolution of 1.9°x2.5° and averaged for the 2004-2006 period. The H<sub>2</sub>O isotopologues a-priori data are averages obtained from the isotopologue incorporated global general circulation model LMDZ (Risi et al., 2012).



Together with the gaseous species, surface skin and atmospheric temperatures are also retrieved simultaneously. As a-priori atmospheric temperature profiles, we use the EUMETSAT IASI L2 temperature profiles distributed by the EPS Ground Segment, which are updated for each retrieval. To constrain the a-priori variability, we consider typical variations of 0.25 K for the atmospheric temperature profile, except for the lowermost atmospheric grid point, where variations of 1 K are allowed for. The surface skin temperature retrieval is not constrained.

For the radiative transfer calculations the spectroscopic line parameters are taken from HITRAN 2012 database (Rothman et al., 2013) for all the gases, except for the H<sub>2</sub>O isotopologues. For the latter we use an improved spectroscopy based on HITRAN 2012, but modifying the line intensities (S) for the HDO absorption signatures by +10% (Schneider et al., 2016). This modification is introduced to correct the bias documented in the IASI HDO products reported by Schneider et al. (2015).

Ocean emissivities are calculated according to Masuda et al. (1988) for three different wavenumbers enveloping the spectral retrieval range, while emissivities at land are taken from the Global Infrared Land Surface Emissivity Database (Seemann et al., 2008) provided as monthly means by the University of Wisconsin in Madison (<http://cimss.ssec.wisc.edu/iremisis/>). The assignment of ground altitude is done using the Global 30 Arc-Second Elevation Dataset (GTOPO30, <http://eros.usgs.gov/elevation-products>), in agreement with August et al. (2012). Note that the PROFFIT-nadir retrieval code does not consider the backscatter of solar light at the Earth's surface, but this is not critical for simulating the radiances below 2000 cm<sup>-1</sup>.

In this study we only consider cloud-free scenes, based on EUMETSAT L2 cloud products. For details about the EUMETSAT IASI cloud screening strategy, refer to August et al. (2012) and the Products User Guide (EUM/OPSEPS/MAN/04/0033, EUMETSAT).

### 2.3 Vertical resolution and sensitivity

The vertical structures that are detectable by the IASI sensor are given by the averaging kernel matrix ( $\mathbf{A}$ , avks) obtained in the retrieval procedure. The rows of this matrix describe the altitude regions that mainly contribute to the retrieved target gas VMR profile and, thus, the vertical distribution of the IASI sensitivity. For  $\mathbf{x}$  being the actual atmospheric state (the actual trace gas profile) and  $\mathbf{x}_a$  the a-priori state it is:

$$\hat{\mathbf{x}} = \mathbf{A}(\mathbf{x} - \mathbf{x}_a) + \mathbf{x}_a + \mathbf{x}_\epsilon \quad (1)$$

Here  $\hat{\mathbf{x}}$  is the retrieved state and  $\mathbf{x}_\epsilon$  are the retrieval errors (see Sect. 2.4).

Figure 2 shows the rows of  $\mathbf{A}$  for typical CH<sub>4</sub> and N<sub>2</sub>O observations over ocean pixels in the tropics and polar regions in winter and summer. Since we are applying a strong regularisation on the CH<sub>4</sub> and N<sub>2</sub>O retrieval, the estimated response of IASI to the real atmospheric variability of CH<sub>4</sub> and N<sub>2</sub>O is almost the same for all altitudes, i.e. all the row avks have almost the same shape and peak at almost the same altitude. As observed in Fig. 2, the IASI sensitivity shows a latitudinal dependency and a weak seasonal dependency. The sensitivity is best in the upper troposphere, i.e.  $\approx 8$  km in polar regions and  $\approx 14$  km in tropics both in summer and winter (intermediate altitudes in middle latitudes, not shown). The full width at half maximum (FWHM) of the row kernels is about 12 km for the tropics and about 10 km for polar latitudes. The kernels indicate



that the MUSICA/IASI retrieval strategy is able to provide CH<sub>4</sub> and N<sub>2</sub>O global distributions of the upper troposphere, which is consistent with the sensitivities obtained by other IASI CH<sub>4</sub> retrievals (e.g. Crevoisier et al., 2013; Xiong et al., 2013).

## 2.4 Theoretical error estimation

The theoretical error estimations are based on evaluating the error covariance matrices,  $\mathbf{S}_\epsilon$ , for each uncertainty source considered. Following the formalism given by (Rodgers, 2000),  $\mathbf{S}_\epsilon$ , is calculated as:

$$\mathbf{S}_\epsilon = \mathbf{G}\mathbf{K}_p\mathbf{S}_{\epsilon,p}\mathbf{K}_p^T\mathbf{G}^T \quad (2)$$

Here  $\mathbf{G}$  is the gain matrix sampling the changes in the retrieved VMR profile,  $\hat{x}$ , for changes at the spectral bin  $y$ ,  $\mathbf{K}_p$  is the parameter Jacobian sampling the changes at the spectral bin  $y$  for changes in the parameter  $p$ , and  $\mathbf{S}_{\epsilon,p}$  is the uncertainty covariance matrix for the uncertainty of  $p$ . We calculate the parameter Jacobians  $\mathbf{K}_p$  for the error source parameters as listed in Table 1. The calculation consists in simulating two spectra using different values of the parameter  $p$ . Then, the differences between the two simulated spectra are divided by the difference applied in the parameter  $p$ .

The different  $\mathbf{S}_{\epsilon,p}$  are given in Table 1. As instrumental errors we consider (i) an conservative IASI radiometric noise of  $2 \times 10^{-2} \mu\text{W}/\text{cm}^2\text{srcm}^{-1}$  (Clerbaux et al., 2009), which corresponds to a measurement noise of 5% (noise-to-signal ratio), and (ii) a deviation in the observing geometry (swath angle) of 0.01 rad. Regarding to model parameters, we assume uncertainties for (i) the surface skin temperature (2 K) and atmospheric temperature profile (2 K between 0-2 km, and 1 K above) in agreement with August et al. (2012), (ii) the ground altitude (20 m) since the IASI pixels may cover complex terrain, (iii) the surface emissivity (1%), and (iv) the spectroscopic parameters (line intensity and pressure-broadening parameter) of 2% for CH<sub>4</sub> and N<sub>2</sub>O. For the major interfering species, the water vapour isotopologues, we assume an uncertainty of 1% in the line intensity parameter and an uncertainty of 5% in the pressure broadening parameter. These error values are in concordance with those reported in the HITRAN database (Rothman et al., 2009). Finally, to account for the humidity interference (so-called cross-dependence on humidity) we assume a variation of 100% of the water vapour isotopologues concentrations.

The error patterns or error vertical profiles are calculated as the square root of the diagonal of the error covariance matrix  $\mathbf{S}_\epsilon$  for each uncertainty source. Figure 3 shows the estimated error profiles. Because we apply a very strong constraint to the shape of the CH<sub>4</sub> and N<sub>2</sub>O profiles, the errors only weakly depend on the altitude. Note that the total random error is estimated as the root-squares-sum of the measurement noise, the cross dependency on humidity, and all the parameter errors, except for spectroscopy.

The error budgets for MUSICA/IASI CH<sub>4</sub> and N<sub>2</sub>O products are very similar. The total random error reaches about 2% and is dominated by uncertainties in the atmospheric temperature profile, the measurement noise and spectral interferences with the strong spectral signatures of H<sub>2</sub>O (cross-dependence on humidity). For more humid tropical conditions it can be even by a factor of 1.5 larger (Fig. 3 is representative for a typical mid-latitude scenario), which reveals the importance of retrieving the CH<sub>4</sub> and N<sub>2</sub>O observations simultaneously with H<sub>2</sub>O. The spectroscopic parameter uncertainties provide errors of 2%, which is mainly due to the uncertainties in the line intensity parameters of CH<sub>4</sub> and N<sub>2</sub>O. Uncertainties in the spectroscopic parameter of the water vapour isotopologues do not significantly contribute to the CH<sub>4</sub> and N<sub>2</sub>O errors.



## 2.5 Dependence on the CH<sub>4</sub> and N<sub>2</sub>O a-priori profiles

The here presented CH<sub>4</sub> and N<sub>2</sub>O retrievals are made on a logarithmic scale with a very strong constraint on the shape of the profiles and we use a single a-priori for all retrievals. The CH<sub>4</sub> and N<sub>2</sub>O a-priori profiles are shown in Fig. 4(a) as solid cyan and green lines, respectively. If we assume linearity, the a-priori and the averaging kernel fully describe the characteristics of our data. We can assimilate the remote sensing data characteristics to any model data (or vertically resolved in-situ data) by applying the averaging kernel to the model data (or in-situ data) in analogy to Eq. (1):

$$\hat{m} = \mathbf{A}(m - x_a) + x_a \quad (3)$$

Here  $m$  is the modeled atmospheric state (or the state as measured by vertically high resolving in-situ instruments) and  $\hat{m}$  the smoothed model state (or the smoothed in-situ state) that has the same characteristics as the remote sensing product  $\hat{x}$ . According to Eqs. (1) and (3) we can calculate the smoothed state for any other a-priori state simply by adding  $(\mathbf{A} - \mathbb{I})(x_a - x_{a,new})$  to  $\hat{x}$  and  $\hat{m}$ , whereby  $x_{a,new}$  is the new a-priori state and  $\mathbb{I}$  an identity matrix.

However, we have to be aware that all the here mentioned operations assume linearity, i.e. it is assumed that  $\mathbf{A}$  does not depend on  $\hat{x}$ . This is actually not true, because strictly speaking  $\mathbf{A}$  is calculated for the retrieved state  $\hat{x}$  and might differ for a slightly different  $\hat{x}$ , which would be obtained by using a new a-priori state. In order to estimate the effect of the non-linearities we test the effect of changing the a-priori data for a typical mid-latitude and polar retrieval. Please recall that we use a low-latitude climatology as single a-priori for all retrievals, so the impact of an inadequate a-priori is statistically larger at middle or high latitudes than at low latitudes. For the typical mid-latitude retrieval we change the a-priori to a mid-latitude climatology (depicted in Fig. 4(a) as dashed blue and dark yellow lines for CH<sub>4</sub> and N<sub>2</sub>O, respectively) and for the typical polar retrieval we change the a-priori to a polar climatology (depicted in Fig. 4(a) as dotted navy blue and dark green lines for CH<sub>4</sub> and N<sub>2</sub>O, respectively). We use two methods for determining the retrieval results with the new a-priori: firstly, we assume linearity and add  $(\mathbf{A} - \mathbb{I})(x_a - x_{a,new})$  to the original retrieval states and, secondly, we perform full retrievals using the new a-priori, thereby considering eventual non-linearities. The difference between the two methods is a good estimate for the importance of non-linearities. These differences are depicted in the two right panels of Fig. 4 (panel (b) for the mid-latitude example and panel (c) for the polar example). For the mid-latitudes the differences are smaller than 0.1% throughout the troposphere. For the polar regions it is a bit larger, but still within 0.5% throughout the troposphere.

If we used a varying a-priori we would also need to work with Eq. (3) before comparing remote sensing with model or in-situ data. However, with a varying a-priori we can better consider seasonal or latitudinal climatologies. Then the a-priori state would statistically be closer to the actual atmospheric state. This means that in average  $x - x_a$  (and similarly  $m - x_a$ ) is smaller for a varying a-priori than for a single a-priori, consequently non-linearities would be of less importance (statistically speaking, because there still might be individual situations where the atmospheric state significantly differs from the climatological state).



### 3 Combination of the N<sub>2</sub>O and CH<sub>4</sub> retrieval products

In this section we present a combination of the N<sub>2</sub>O and CH<sub>4</sub> retrieval products, with the final objective to generate a more precise CH<sub>4</sub> product.

#### 3.1 Motivation

- 5 When aiming at precise CH<sub>4</sub> observations from space-based platforms, a successful method to reduce CH<sub>4</sub> errors is to combine the retrieved CH<sub>4</sub> observations a-posteriori with the co-retrieved N<sub>2</sub>O estimates (Razavi et al., 2009; Worden et al., 2012). This approach relies on two key issues: (i) CH<sub>4</sub> and N<sub>2</sub>O retrievals similarly behave to many uncertainties sources, such as temperature, clouds and emissivity; and (ii) the atmospheric N<sub>2</sub>O concentrations are rather stable and have continuously grown at an almost constant rate (Stocker et al., 2013).
- 10 In analogy to Eq. (1) we can work with the retrieved N<sub>2</sub>O and CH<sub>4</sub> state vectors in the logarithmic scale and write:

$$\begin{aligned}\hat{\mathbf{x}}_{\text{N}_2\text{O}} &= \mathbf{A}_{\text{N}_2\text{O}}(\mathbf{x}_{\text{N}_2\text{O}} - \mathbf{x}_{a,\text{N}_2\text{O}}) + \mathbf{x}_{a,\text{N}_2\text{O}} + \mathbf{x}_{\epsilon,\text{N}_2\text{O}} \\ \hat{\mathbf{x}}_{\text{CH}_4} &= \mathbf{A}_{\text{CH}_4}(\mathbf{x}_{\text{CH}_4} - \mathbf{x}_{a,\text{CH}_4}) + \mathbf{x}_{a,\text{CH}_4} + \mathbf{x}_{\epsilon,\text{CH}_4}\end{aligned}\quad (4)$$

Here  $\hat{\mathbf{x}}$  is the retrieved state vector,  $\mathbf{x}_a$  the a-priori state vector,  $\mathbf{x}$  the state vector that describes the actual atmosphere and  $\mathbf{x}_{\epsilon} = \mathbf{G}\mathbf{K}_p\mathbf{p}_{\epsilon}$  captures the errors due to uncertainties in the retrieval parameters  $\mathbf{p}_{\epsilon}$  (for instance, uncertainties in temperature or spectroscopic parameters). As before, the matrices  $\mathbf{A}$  are the averaging kernels.

If we now define the combined product as the difference between the state vectors (difference in the logarithmic scale), we get:

$$\hat{\mathbf{x}}_{\text{CH}_4} - \hat{\mathbf{x}}_{\text{N}_2\text{O}} = \mathbf{x}_{a,\text{CH}_4} - \mathbf{x}_{a,\text{N}_2\text{O}} + \mathbf{A}_{\text{CH}_4}(\mathbf{x}_{\text{CH}_4} - \mathbf{x}_{a,\text{CH}_4}) - \mathbf{A}_{\text{N}_2\text{O}}(\mathbf{x}_{\text{N}_2\text{O}} - \mathbf{x}_{a,\text{N}_2\text{O}}) + \mathbf{x}_{\epsilon,\text{CH}_4} - \mathbf{x}_{\epsilon,\text{N}_2\text{O}}\quad (5)$$

The idea is that (i) the error of this combined product  $\{\mathbf{x}_{\epsilon,\text{CH}_4} - \mathbf{x}_{\epsilon,\text{N}_2\text{O}}\}$  is much smaller than the errors in the individual products  $\{\mathbf{x}_{\epsilon,\text{CH}_4}$  or  $\mathbf{x}_{\epsilon,\text{N}_2\text{O}}\}$ , and (ii) as N<sub>2</sub>O shares the dynamical variations of CH<sub>4</sub> in the tropopause region, the combined product has a weaker dependency on the tropopause altitude and potentially an improved representativeness of source/sink signals.

#### 3.2 Theoretical treatment of the combined CH<sub>4</sub> product

By a simple matrix multiplication we can make a transformation for the  $\{\ln[\text{N}_2\text{O}], \ln[\text{CH}_4]\}$  space into the  $\{\frac{\ln[\text{CH}_4] + \ln[\text{N}_2\text{O}]}{2}, \ln[\text{CH}_4] - \ln[\text{N}_2\text{O}]\}$  space. This transformation between basis systems has been discussed in detail for water vapour isotopologue states in Schneider et al. (2012) and the same approach can be applied for the N<sub>2</sub>O and CH<sub>4</sub> states. The transformation matrix  $\mathbf{P}$  is:

$$\mathbf{P} = \begin{pmatrix} \frac{1}{2}\mathbb{I} & \frac{1}{2}\mathbb{I} \\ -\mathbb{I} & \mathbb{I} \end{pmatrix}\quad (6)$$

Here, the four matrix blocks have the dimension  $(nol \times nol)$ , and  $\mathbb{I}$  stands for an identity matrix.



### 3.2.1 Theoretical error estimation

The error covariance matrix for the transformed states can be easily calculated in analogy to Eq. (2):

$$\mathbf{S}'_{\epsilon} = \mathbf{P}\mathbf{G}\mathbf{K}_p\mathbf{S}_{\epsilon,p}\mathbf{K}_p^T\mathbf{G}^T\mathbf{P}^T = \begin{pmatrix} \mathbf{S}'_{\epsilon 11} & \mathbf{S}'_{\epsilon 12} \\ \mathbf{S}'_{\epsilon 21} & \mathbf{S}'_{\epsilon 22} \end{pmatrix} \quad (7)$$

There are four matrix blocks with the dimension ( $noI \times noI$ ). The error covariances for the combined product  $\hat{\mathbf{x}}_{CH_4} - \hat{\mathbf{x}}_{N_2O}$  are collected in the matrix block  $\mathbf{S}'_{\epsilon 22}$  (for more details and discussion please refer to Sect. 4.1.2 of Schneider et al., 2012).

The bottom panel of Fig. 3 shows the square root values of the diagonal of the matrix block  $\mathbf{S}'_{\epsilon 22}$  obtained for the different uncertainty sources. It demonstrates that in the combined product the impact of many uncertainty sources is indeed significantly reduced: for atmospheric temperatures, cross dependencies from water vapour, surface temperature, etc. These are the uncertainty sources that are common for  $N_2O$  and  $CH_4$ . The uncertainty due to measurement noise is of course increased, because the measurement noise of  $N_2O$  and  $CH_4$  are independent uncertainty sources and in the combined products the errors are larger than in the individual products. However, the total random error is significantly reduced by a factor of 2 (from 2% to less than 1%). Measurement noise and uncertainties in the atmospheric temperature profiles are the leading error sources.

In the combined product the error due to uncertainties of spectroscopic parameter is increased, because we assume that the uncertainties in the spectroscopic parameters of  $N_2O$  and  $CH_4$  are independent.

### 3.2.2 Dependence on the a-priori profile

As already mentioned in several sections of the paper we use a single  $N_2O$  and  $CH_4$  a-priori state for all the retrievals, which are averaged from a low-latitude climatology. In particular for higher latitudes this a-priori state might be significantly different from the retrieved state. As a consequence non-linearities can become important. In Sect. 2.5 we describe how the importance of such non-linearities can be estimated for the individual  $N_2O$  and  $CH_4$  products. The respective estimation for the combined product is depicted as navy blue line in Fig. 4 (left panel for mid-latitudes and right panel for polar latitudes). We found that the non-linearity can cause misinterpretations in the troposphere of 0.06% and 0.50% for a typical mid-latitude and polar situation, respectively.

### 3.3 Possibility for generating a high quality $CH_4$ product

Since  $N_2O$  is relatively stable it might be possible that the horizontal and vertical  $N_2O$  distribution is reasonably well captured by atmospheric models. For example, by assimilating high quality  $N_2O$  observations at a few reference locations, it might in the future become possible to generate reliable three dimensional  $N_2O$  fields on a global scale. If  $\mathbf{x}_{N_2O}$  is reasonably well known on a global scale, we could add  $\mathbf{A}_{N_2O}(\mathbf{x}_{N_2O} - \mathbf{x}_{a,N_2O}) + \mathbf{x}_{a,N_2O}$  to Eq. (5), thereby reconstructing a  $CH_4$  product from the combined product. This reconstructed  $CH_4$  product would have an improved precision (see Fig. 3).



In the following and for simplicity we assume that  $\mathbf{x}_{\text{N}_2\text{O}} = \mathbf{x}_{a,\text{N}_2\text{O}}$ , which means that we calculate an a-posteriori corrected  $\text{CH}_4$  product ( $\hat{\mathbf{x}}'_{\text{CH}_4}$ ) as:

$$\hat{\mathbf{x}}'_{\text{CH}_4} = (\hat{\mathbf{x}}_{\text{CH}_4} - \hat{\mathbf{x}}_{\text{N}_2\text{O}}) + \mathbf{x}_{a,\text{N}_2\text{O}} \quad (8)$$

Please be aware that here we use a very simple  $\mathbf{x}_{a,\text{N}_2\text{O}}$  assumption (temporarily and horizontally not varying data), which disregards the horizontal, vertical and seasonal variations of  $\text{N}_2\text{O}$ . In this context the here used  $\hat{\mathbf{x}}'_{\text{CH}_4}$  is not a pure  $\text{CH}_4$  product, instead it contains combined information on  $\text{CH}_4$  and  $\text{N}_2\text{O}$  variations. In the following we will refer to  $\hat{\mathbf{x}}'_{\text{CH}_4}$  as the product "CH<sub>4</sub> combined with N<sub>2</sub>O".

## 4 Empirical validation of the MUSICA/IASI products

### 4.1 CH<sub>4</sub> and N<sub>2</sub>O HIPPO vertical profiles

The project HIPPO (<http://hippo.ucar.edu/>) investigated carbon cycle and greenhouse gases by sampling the atmosphere from approximately 67°S to 80°N mostly over the Pacific Ocean, from the surface to 14 km (~ 150-300 hPa) and spanning all the seasons between 2009-2011 (Wofsy et al., 2011). In total five measurement missions were conducted aboard HIAPER, a modified Gulfstream-V (G-V) aircraft: January 2009 (HIPPO1), November 2009 (HIPPO2), March/April 2010 (HIPPO3), June 2011 (HIPPO4) and August/September 2011 (HIPPO5). During these missions,  $\text{CH}_4$  and  $\text{N}_2\text{O}$  in-situ measurements were performed using a QCLS (quantum-cascade laser spectrometer) instrument at 1Hz frequency with a precision of 0.5 ppbv and 0.09 ppbv for  $\text{CH}_4$  and  $\text{N}_2\text{O}$ , respectively, and an accuracy of 1.0 ppbv for both trace gases (Santoni et al., 2014). Here, we focus on HIPPO1 and HIPPO5 missions in order to span the maximal/minimal  $\text{CH}_4$  and  $\text{N}_2\text{O}$  annual concentrations, and from these, we only consider the research flights and disregard measurements taken during HIPPO training phases.

Figure 5 displays the geographical distribution of the HIPPO flights during the HIPPO1 and HIPPO5 missions as well as the latitudinal distribution of  $\text{CH}_4$  and  $\text{N}_2\text{O}$  vertical profiles (for HIPPO1 flights only). The rightmost panel shows the "CH<sub>4</sub> combined with N<sub>2</sub>O" profile product, where the high variability observed in the tropopause region is partly dampened, because of  $\text{CH}_4$  and  $\text{N}_2\text{O}$  showing similar dependencies of the tropopause altitude.

For the HIPPO data the "CH<sub>4</sub> combined with N<sub>2</sub>O" product is calculated in analogy to Eq. (8):

$$\mathbf{h}'_{\text{CH}_4} = (\mathbf{h}_{\text{CH}_4} - \mathbf{h}_{\text{N}_2\text{O}}) + \mathbf{h}_{a,\text{N}_2\text{O}} \quad (9)$$

Whereby  $\mathbf{h}$  are the state vectors containing the HIPPO data and  $\mathbf{h}_{a,\text{N}_2\text{O}}$  is the same as  $\mathbf{x}_{a,\text{N}_2\text{O}}$ , but interpolated to the vertical grid that corresponds to the HIPPO measurements. Note that the calculations are made on a logarithmic scale.

### 4.2 Validation Strategy

IASI and HIPPO observations are sensing areas of different size with different acquisition times, thereby appropriate spatial and temporal collocation criteria have to be defined to ensure a feasible inter-comparison. Similarly to previous studies using



HIPPO aircraft observations (Wecht et al., 2012; Xiong et al., 2013), each HIPPO vertical profile (covering  $\sim 220$  km,  $2.2^\circ$  latitude, and  $\sim 20$  minutes) is characterised by a mean location (latitude and longitude) and a mean time. Then, we consider all the IASI observations within the box  $\pm 2^\circ$  latitude/longitude centred at each HIPPO mean location and  $\pm 12$ h around every HIPPO mean profile. In order to quantify the real spatial resolution captured by the MUSICA/IASI  $\text{CH}_4$  and  $\text{N}_2\text{O}$  products, the IASI-HIPPO comparison will be performed (i) considering all the valid IASI retrievals within the validation box, so that all the IASI variability is kept, and (ii) averaging all the valid IASI retrievals within the validation box, so that the IASI noise is reduced and the results are more comparable to the typical spatial resolution of the global climate models.

Another key issue when validating remote-sensing vertical profiles is to take into account the low vertical resolution and limited sensitivity of these data. For this purpose, the vertically highly-resolved HIPPO  $\text{CH}_4$  and  $\text{N}_2\text{O}$  profiles ( $h_{\text{CH}_4}$  and  $h_{\text{N}_2\text{O}}$ ) are degraded applying the averaging kernels of the vertically poorly resolved profiles obtained from IASI retrievals:

$$\begin{aligned}\hat{h}_{\text{N}_2\text{O}} &= \mathbf{A}_{\text{N}_2\text{O}}(h_{\text{N}_2\text{O}} - \mathbf{x}_{a,\text{N}_2\text{O}}) + \mathbf{x}_{a,\text{N}_2\text{O}} \\ \hat{h}_{\text{CH}_4} &= \mathbf{A}_{\text{CH}_4}(h_{\text{CH}_4} - \mathbf{x}_{a,\text{CH}_4}) + \mathbf{x}_{a,\text{CH}_4}\end{aligned}\quad (10)$$

When comparing  $\hat{h}_{\text{CH}_4}$  and  $\hat{h}_{\text{N}_2\text{O}}$  with the corresponding IASI retrievals the different sensitivities are accounted for. Note that, the calculations are made on a logarithmic scale.

Because the HIPPO aircraft profiles only reach 14 km, beyond this altitude they have to be extended before applying Eq. (10) in order to span the vertical range covered by IASI retrieval scheme. For this purpose we use the monthly and zonally averaged  $\text{CH}_4$  and  $\text{N}_2\text{O}$  climatology from the Atmospheric Chemistry Experiment-Fourier Transform Spectrometer (ACE-FTS) observations between February 2004-February 2009 (Jones et al., 2012). The ACE-FTS climatological profiles are computed by using ACE-FTS version 2.2 and are provided as averages of  $5^\circ$  latitudinal bands and from 500 to 0.1 hPa. Since the ACE-FTS climatology presents some latitudinal gaps, specially in the tropics, we have averaged these climatological profiles in bands of  $30^\circ$  covering from  $90^\circ\text{N}$  to  $90^\circ\text{S}$  and distinguishing the seasons. Consequently, the smoothed HIPPO profiles are a combination of two experiments: the HIPPO in-situ profiles and the averaged ACE-FTS climatology.

The IASI and HIPPO inter-comparison can only be performed for the altitude regions that are sufficiently well detectable by IASI, i.e. the  $\text{CH}_4$  and  $\text{N}_2\text{O}$  VMR concentrations in the upper troposphere (see Fig. 2 and corresponding discussion). In this study we do all the comparisons for the altitude of 10 km. This is a good compromise between the altitude of the IASI maximum sensitivity and the number of available HIPPO observations. In order to ensure that the reference data are mainly based on HIPPO observations, we only consider the HIPPO flights with  $\text{CH}_4$  and  $\text{N}_2\text{O}$  records up to at least 10 km (88 out of 304 valid aircraft profiles during HIPPO1 and HIPPO5).

### 4.3 Comparison between MUSICA/IASI and HIPPO products

Figure 6 summarizes the straightforward comparison of the MUSICA/IASI  $\text{CH}_4$  and  $\text{N}_2\text{O}$  retrievals with the corresponding HIPPO records smoothed by the IASI avks. The MUSICA/IASI products show a fairly good agreement with the in-situ data: correlation coefficient (R) of 0.51 and 0.60 for  $\text{CH}_4$  and  $\text{N}_2\text{O}$ , respectively, when considering all the IASI-HIPPO pairs. The agreement significantly increases for the  $2^\circ \times 2^\circ$  averages (R of larger than 0.70). The scatter of the differences between



MUSICA/IASI and HIPPO data (Table 2), which can be used as a conservative estimate of the IASI error. It is about 3% (2% for  $2^\circ \times 2^\circ$  averages) for both GHGs, meaning a scatter in absolute values of 38.2 ppbv (32.1 ppbv for  $2^\circ \times 2^\circ$  averages) for  $\text{CH}_4$  and 8.7 ppbv (6.9 ppbv for  $2^\circ \times 2^\circ$  averages) for  $\text{N}_2\text{O}$ . These values are in good agreement with the theoretical error estimation as shown in section 2.4, which documents the confidence of the theoretical assessment. The IASI-HIPPO inter-comparison also indicates that while the IASI  $\text{N}_2\text{O}$  retrievals do not show any significant bias, the  $\text{CH}_4$  estimates are biased high by about 2%. According to our error estimation, this bias can be explained by the spectroscopic parameters used in the MUSICA/IASI retrievals (HITRAN 2012 database). Note that as statistical estimators of MUSICA/IASI's bias and precision we have computed the median, the semi-distance between the percentiles 84.1<sup>th</sup> and 15.9<sup>th</sup> of the difference between IASI and HIPPO (IP68), and the standard deviation. The former two values are less sensitive to the presence of outliers and extreme values, allowing for more robust conclusions on the inter-comparison result.

There already have been empirical validation studies of IASI  $\text{CH}_4$  products obtained by other research groups. For example, Xiong et al. (2013) found a low bias to HIPPO aircraft profiles of -1.69% (approximately 30 ppbv) with a residual scatter of 1.13% (approximately 23 ppbv) in the integrated 300-374 hPa layer for a collocation window with a distance of 200 km. In a study limited to the tropics Crevoisier et al. (2013) compared IASI and CARIBIC aircraft measurements of  $\text{CH}_4$  at 11 km for  $4^\circ \times 4^\circ$  averages and found a high bias of 7 ppbv (approximately 0.5%) with a scatter of 13 ppbv (approximately 0.8%).

Concerning  $\text{N}_2\text{O}$ , Masiello et al. (2016) has recently shown that  $\text{N}_2\text{O}$  global distributions could be obtained for each single IASI IFOV with a theoretical precision of better than 1-2%. To our knowledge our study is the first where an extensive IASI  $\text{N}_2\text{O}$  dataset is empirically validated, and it is interesting to see that our empirical validation results are close to the theoretical estimations of Masiello et al. (2016).

The rightmost panels of Fig. 6 empirically confirm that the a-posteriori combination considering the co-retrieved  $\text{N}_2\text{O}$  estimates can successfully be used to reduce common errors in the  $\text{CH}_4$  and  $\text{N}_2\text{O}$  retrievals and part of the effect of the tropopause shift, which importantly affects the upper tropospheric  $\text{CH}_4$  and  $\text{N}_2\text{O}$  concentrations that are observed by the remote sensor IASI (recall Fig. 2). The coefficients R for the correlation between the MUSICA and HIPPO " $\text{CH}_4$  combined with  $\text{N}_2\text{O}$ " data are 0.86 and 0.89 when considering all the IASI observations and the  $2^\circ \times 2^\circ$  averages, respectively, which are significantly higher than the correlations of the individual  $\text{CH}_4$  and  $\text{N}_2\text{O}$  data. Furthermore, there is also a noticeable decrease in the bias and the scatter of the combined product (see Table 2). Therefore, when correcting the  $\text{CH}_4$  retrievals with the co-retrieved  $\text{N}_2\text{O}$  values according to Eq. (8), IASI can provide very robust data and is able to detect upper tropospheric patterns on rather small scales (every morning, every evening and globally at all cloud-free scenarios).

The differences between the MUSICA/IASI and HIPPO data have been analysed as a function of the different parameters, such as the latitude or the HIPPO missions, which were taken in different seasons and during different years. These analyses are summarised in Fig. 7. We find no significant differences between the two HIPPO missions and no significant dependency on latitude. In particular for the " $\text{CH}_4$  combined with  $\text{N}_2\text{O}$ " product the IASI and the HIPPO data show a very uniform agreement (see Fig. 7(c)).



## 5 Global distribution of the MUSICA/IASI products

The previous theoretical and experimental quality assessment points out that the CH<sub>4</sub> and N<sub>2</sub>O estimates for individual IASI observations are much more noisy than for 2°x2° averages. In order to identify reliable CH<sub>4</sub> and N<sub>2</sub>O patterns on a global scale we should consider the averages. The **combined** product has also a good precision without averaging, however for consistency reasons in the following we also use the 2°x2° averages. Figure 8 illustrates the coverage at ≈350-300 hPa for a morning observation in boreal winter and summer. These global maps can be produced from MetOp/IASI spectra every day and for each morning and evening overpass. The areas with missing data are the ones that are identified by EUMETSAT as cloudy or did not pass the MUSICA MetOp/IASI spectral fit quality criterion (for more details see Schneider et al., 2016). The obtained CH<sub>4</sub> and N<sub>2</sub>O distributions show the well known latitudinal gradient with a tendency to higher concentrations in low latitudes than in high latitudes. In addition, the well known seasonal cycle can be observed: the concentrations are higher in summer than in winter. This seasonal cycle is more pronounced for CH<sub>4</sub> than for N<sub>2</sub>O and in the northern hemisphere than in the southern hemisphere due to the location of the stronger emission sources (e.g. Huang et al., 2008; Bousquet et al., 2011; Worden et al., 2012; Stocker et al., 2013, and references therein). Highest CH<sub>4</sub> concentrations are found in the northern hemispheric summer.

The global maps for the combined product are shown in the bottom panels of Fig. 8. It should be noted that although the seasonal signals captured by the CH<sub>4</sub> product and the product "CH<sub>4</sub> combined with N<sub>2</sub>O" seem to be comparable, both products present slightly different global patterns. For example, the combined product exhibits a more defined latitudinal gradient and the regional features as seen during boreal summer over the southeast Asia and India in the original CH<sub>4</sub> product, almost disappear in the global maps of the combined product.

## 6 IASI-A and IASI-B consistency assessment

Since the end of 2012 two IASI sensors (IASI-A and IASI-B) are in operation simultaneously on-board the EUMETSAT MetOp-A and MetOp-B meteorological satellites. Their respective overpasses take place typically within 30 minutes, which offers very good possibilities to cross-validate the IASI-A and -B products (Schneider et al., 2016). The continuous inter-comparison of both sensors also offers important diagnostics for identifying instrumental issues and for documenting the long-term temporal stability of IASI records (García et al., 2016).

Figure 9 depicts an example of the IASI-A and IASI-B consistency assessment on global scale for 16.08.2014 (left columns for the morning overpass and right columns for the evening overpass) with IASI-A and IASI-B observations being paired within 0.25°x0.25° boxes. We find a reasonable global consistency of the IASI-A and IASI-B products, thereby the CH<sub>4</sub> and N<sub>2</sub>O observations from both sensors could be merged into a unique IASI database. A particular good consistency is found for the combined product, which confirms the feasibility of the a-posteriori combination of CH<sub>4</sub> with the co-retrieved N<sub>2</sub>O.



## 7 EUMETSAT/IASI CH<sub>4</sub> and N<sub>2</sub>O products

The EUMETSAT Polar System (EPS)/Core Ground Segment has operationally provided the IASI Level 2 trace gas products since 2008. In addition to humidity and temperature profiles among other parameters, EUMETSAT IASI L2 include total column amounts (TC) of CH<sub>4</sub> and N<sub>2</sub>O. They are retrieved using an inversion algorithm based on artificial neuronal networks (ANN) with an expected theoretical uncertainty between 10-20% (August et al., 2012, and references therein). These products benefit from the improvements in the ANN design introduced by the different IASI processors (Version 4 -V4-, Version 5 -V5-, and Version 6 -V6-), but they have not been specifically optimised and still are considered as aspirational products.

To compare the EUMETSAT CH<sub>4</sub> and N<sub>2</sub>O TC to the HIPPO in-situ data, the total column-averaged dry air mole fractions of CH<sub>4</sub> (XCH<sub>4</sub>) and N<sub>2</sub>O (XN<sub>2</sub>O) are calculated dividing the respective TC by the dry pressure column (DPC) above each IASI ground pixel. The DPC is calculated converting the ground pressure to column air concentration as follows:

$$DPC = \frac{P_s}{m_{dryair}} \cdot g(\varphi) - \frac{m_{H_2O}}{m_{dryair}} \cdot H_2O_{col} \quad (11)$$

where  $P_s$  is the surface pressure at ground level,  $m_{dryair}$  the molecular mass of the dry air ( $\approx 28.96 \text{ gmol}^{-1}$ ),  $m_{H_2O}$  the molecular mass of the water vapour ( $\approx 18 \text{ gmol}^{-1}$ ),  $H_2O_{col}$  the water vapour total column amount, and  $g(\varphi)$  the latitude-dependent surface acceleration due to gravity. The ground pressure was taken from the EUMETSAT IASI L2 products.

Similarly to MUSICA/IASI, EUMETSAT/IASI CH<sub>4</sub> and N<sub>2</sub>O products are expected to reflect the concentration variations in the tropopause region, thereby the operational IASI XCH<sub>4</sub> and XN<sub>2</sub>O retrievals are compared to HIPPO VMR records at 10 km. Note that, as the EUMETSAT/IASI CH<sub>4</sub> and N<sub>2</sub>O are estimated using ANN, the averaging kernels are not available and, thus, the HIPPO data can not be smoothed by the corresponding IASI avks.

Figure 10 summarizes the comparison between EUMETSAT/IASI and HIPPO, where the two HIPPO mission have to be considered separately, since the IASI V5 (introduced in September 2010) significantly improved the quality of the IASI CH<sub>4</sub> and N<sub>2</sub>O observations (García et al., 2013). Considering only the IASI V5 data (i.e. HIPPO5), the agreement between EUMETSAT/IASI and HIPPO data is moderately good (R of 0.67 and 0.60 for XCH<sub>4</sub> and XN<sub>2</sub>O, respectively).

Interestingly, we can also combine the EUMETSAT L2 XN<sub>2</sub>O and XCH<sub>4</sub> and thereby generate a combined product according to Eq. (8) with significantly improved precision. For the correlation between the combined EUMETSAT L2 product and the respective HIPPO product we calculated a correlation coefficient R of 0.79 (see right panel in Fig. 10).

## 8 Conclusions

Monitoring CH<sub>4</sub> and N<sub>2</sub>O by thermal nadir remote sensing is a challenging task. CH<sub>4</sub> and N<sub>2</sub>O vary only weakly. In the thermal nadir radiances the spectral signatures of these weak variations are rather difficult to observe, because they interfere with the strong spectral signatures of the highly variable tropospheric H<sub>2</sub>O amounts. In the last years, the satellite community has made considerable efforts in developing and improving respective retrieval strategies and the scientific discussion is still on-going. In this context, we propose to retrieve N<sub>2</sub>O and CH<sub>4</sub> simultaneously with H<sub>2</sub>O and use the retrieval strategy that has been developed in the framework of the European project MUSICA.



We demonstrate that the MUSICA/IASI  $\text{N}_2\text{O}$  and  $\text{CH}_4$  products are representative for the upper troposphere and that their theoretical precision is about 2%. These values are empirically confirmed by comparisons to merged HIPPO/ACE-FTS data. The theoretical estimation identifies the atmospheric temperature considered in the retrieval procedure, the IASI measurement noise and the cross dependency on tropospheric humidity variations as leading error sources.

We present a combined  $\text{CH}_4$  and  $\text{N}_2\text{O}$  retrieval product. We estimate its theoretical precision to be 1% (i.e. much better than for the individual  $\text{CH}_4$  and  $\text{N}_2\text{O}$  products) and the comparison to the HIPPO/ACE-FTS reference data empirically confirms this estimation. Interestingly the a-posteriori combination also works with the EUMETSAT Level 2  $\text{N}_2\text{O}$  and  $\text{CH}_4$  products, suggesting that it can be applied to any  $\text{N}_2\text{O}$  and  $\text{CH}_4$  data that have been simultaneously retrieved from thermal nadir measurements.

A unique potential of IASI is the twice daily global coverage and long-term mission strategy. This paper demonstrates the quality of the MUSICA MetOp/IASI  $\text{CH}_4$  and  $\text{N}_2\text{O}$  products and also briefly discusses respective EUMETSAT L2 products. These products are mainly sensitive to the upper troposphere. In the next step it should be examined to what extent IASI observations of upper tropospheric  $\text{CH}_4$  and  $\text{N}_2\text{O}$  variations can help to investigate the emission source patterns, transport pathways and sinks of  $\text{CH}_4$  and  $\text{N}_2\text{O}$ , and whether the provision of a highly precise product (" $\text{CH}_4$  combined with  $\text{N}_2\text{O}$ ") offers additional benefits for such research purposes.

## 15 9 Data availability

The here presented MUSICA MetOp/IASI data are currently prepared for dissemination in a database. This work has still not finished and currently the data are only available by request to the author.

The HIPPO data are publicly available at <http://hippo.ucar.edu/>. This HIPPO site is maintained by the National Center for Atmospheric Research (NCAR) Earth Observing Laboratory (EOL), which is a laboratory within the National Center for Atmospheric Research (NCAR). NCAR is managed by the University Corporation for Atmospheric Research (UCAR) under sponsorship by the National Science Foundation (NSF).

The EUMETSAT IASI L2 total column amounts of  $\text{CH}_4$  and  $\text{N}_2\text{O}$  are generated by the EUMETSAT Polar System Core Ground Segment and publicly available at the EUMETSAT Data Centre at [www.eumetsat.int](http://www.eumetsat.int).

*Author contributions.* O.E. García coordinated this work and performed the MUSICA MetOp/IASI retrievals for the coincidences with the HIPPO observations and made all the error estimation and the comparative studies (MUSICA MetOp/IASI versus HIPPO and EUMETSAT IASI L2 versus HIPPO). E. Sepúlveda, M. Schneider, A. Wiegele, C. Borger, and F. Hase supported the IASI retrieval and the error estimation activities. M. Schneider set up the MUSICA MetOp/IASI retrieval and developed the combined  $\text{CH}_4$  and  $\text{N}_2\text{O}$  product. A. Wiegele performed the global MUSICA MetOp/IASI retrievals. F. Hase developed the PROFFIT-nadir retrieval code. The manuscript has been prepared with contributions from all co-authors.



- 30 *Acknowledgements.* The research leading to these results has received funding from the European Research Council under FP7/(2007-2013)/ERC Grant agreement n° 256961 (project MUSICA), from the Ministerio de Economía y Competitividad from Spain through the project CGL2012-37505 (project NOVIA), from the Ministerio de Educación, Cultura y Deporte (Programa "José Castillejo", CAS14/00282), and from EUMETSAT under its Fellowship Programme (project VALIASI). Furthermore, we would like to acknowledge the climatological data provided by Atmospheric Chemistry Experiment (ACE), also known as SCISAT, that is a Canadian-led mission mainly supported by the
- 5 Canadian Space Agency, and to the National Science Foundation (NSF) and the National Oceanic and Atmospheric Administration (NOAA), that supported the collection of the original HIPPO data.



## References

- Angelbratt, J., Mellqvist, J., Blumenstock, T., Borsdorff, T., Brohede, S., Duchatelet, P., Forster, F., Hase, F., Mahieu, E., Murtagh, D., Petersen, A. K., Schneider, M., Sussmann, R., and Urban, J.: A new method to detect long term trends of methane (CH<sub>4</sub>) and nitrous oxide (N<sub>2</sub>O) total columns measured within the NDACC ground-based high resolution solar FTIR network, *Atmospheric Chemistry and Physics*, 11, 6167–6183, doi:10.5194/acp-11-6167-2011, 2011.
- 5 August, T., Klaes, D., Schlüssel, P., Hultberg, T., Crapeau, M., Arriaga, A., O’Carroll, A., Coppens, D., Munro, R., and Calbet, X.: IASI on Metop-A: Operational Level 2 retrievals after five years in orbit, *J. Quant. Spectrosc. Radiat. Transfer*, doi:10.1016/j.jqsrt.2012.02.028, 2012.
- Blumstein, D., Chalon, G., Carlier, T., Buil, C., Hébert, P., Maciaszek, T., Ponce, G., Phulpin, T., Tournier, B., and Siméoni, D.: IASI instrument: Technical Overview and measured performances, in: *Proceedings SPIE*, SPIE, Denver, 2004.
- 10 Bousquet, P., Ringeval, B., Pison, I., Dlugokencky, E. J., Brunke, E.-G., Carouge, C., Chevallier, F., Fortems-Cheiney, A., Frankenberg, C., Hauglustaine, D. A., Krummel, P. B., Langenfelds, R. L., Ramonet, M., Schmidt, M., Steele, L. P., Szopa, S., Yver, C., Viovy, N., and Ciais, P.: Source attribution of the changes in atmospheric methane for 2006–2008, *Atmospheric Chemistry and Physics*, 11, 3689–3700, doi:10.5194/acp-11-3689-2011, 2011.
- Clerbaux, C., Boynard, A., Clarisse, L., George, M., Hadji-Lazaro, J., Herbin, H., Hurtmans, D., Pommier, M., Razavi, A., Turquety, S., 15 Wespes, C., and Coheur, P.-F.: Monitoring of atmospheric composition using the thermal infrared IASI/MetOp sounder, *Atmospheric Chemistry and Physics*, 9, 6041–6054, doi:10.5194/acp-9-6041-2009, 2009.
- Cressot, C., Chevallier, F., Bousquet, P., Crevoisier, C., Dlugokencky, E. J., Fortems-Cheiney, A., Frankenberg, C., Parker, R., Pison, I., Scheepmaker, R. A., Montzka, S. A., Krummel, P. B., Steele, L. P., and Langenfelds, R. L.: On the consistency between global and regional methane emissions inferred from SCIAMACHY, TANSO-FTS, IASI and surface measurements, *Atmospheric Chemistry and 20 Physics*, 14, 577–592, doi:10.5194/acp-14-577-2014, 2014.
- Crevoisier, C., Nobileau, D., Fiore, A. M., Armante, R., Chédin, A., and Scott, N. A.: Tropospheric methane in the tropics - first year from IASI hyperspectral infrared observations, *Atmospheric Chemistry and Physics*, 9, 6337–6350, doi:10.5194/acp-9-6337-2009, 2009.
- Crevoisier, C., Nobileau, D., Armante, R., Crépeau, L., Machida, T., Sawa, Y., Matsueda, H., Schuck, T., Thonat, T., Pernin, J., Scott, N. A., and Chédin, A.: The 2007–2011 evolution of tropical methane in the mid-troposphere as seen from space by MetOp-A/IASI, *Atmospheric 25 Chemistry and Physics*, 13, 4279–4289, doi:10.5194/acp-13-4279-2013, 2013.
- Crevoisier, C., Clerbaux, C., Guidard, V., Phulpin, T., Armante, R., Barret, B., Camy-Peyret, C., Chaboureaud, J.-P., Coheur, P.-F., Crépeau, L., Dufour, G., Labonnote, L., Lavanant, L., Hadji-Lazaro, J., Herbin, H., Jacquinet-Husson, N., Payan, S., Péquignot, E., Pierangelo, C., Sellitto, P., and Stubenrauch, C.: Towards IASI-New Generation (IASI-NG): impact of improved spectral resolution and radiometric noise on the retrieval of thermodynamic, chemistry and climate variables, *Atmospheric Measurement Techniques*, 7, 4367–4385, 30 doi:10.5194/amt-7-4367-2014, 2014.
- De Mazière, M., Vigouroux, C., Bernath, P. F., Baron, P., Blumenstock, T., Boone, C., Brogniez, C., Catoire, V., Coffey, M., Duchatelet, P., Griffith, D., Hannigan, J., Kasai, Y., Kramer, I., Jones, N., Mahieu, E., Manney, G. L., Piccolo, C., Randall, C., Robert, C., Senten, C., Strong, K., Taylor, J., Tétard, C., Walker, K. A., and Wood, S.: Validation of ACE-FTS v2.2 methane profiles from the upper troposphere to the lower mesosphere, *Atmospheric Chemistry and Physics*, 8, 2421–2435, doi:10.5194/acp-8-2421-2008, 2008.



- 35 Frankenberg, C., Meirink, J. F., Bergamaschi, P., Goede, A., Heimann, M., Korner, S., Platt, U., van Weele, M., and Wagner, T.: Satellite cartography of atmospheric methane from SCIAMACHY on board ENVISAT: Analysis of the years 2003 and 2004, *Journal of Geophysical Research*, 111, doi:doi:10.1029/2005JD006235, 2006.
- García, O. E., Schneider, M., Hase, F., Blumenstock, T., Wiegeler, A., Sepúlveda, E., and Gómez-Peláez, A.: Validation of the IASI operational CH<sub>4</sub> and N<sub>2</sub>O products using ground-based Fourier Transform Spectrometer: Preliminary results at the Izaña Observatory (28°N, 17°W), *Annals of Geophysics*, 56, 2013.
- 5 García, O. E., Sepúlveda, E., Schneider, M., Hase, F., August, T., Blumenstock, T., Kühl, S., Munro, R., Gómez-Peláez, A. J., Hultberg, T., Redondas, A., Barthlott, S., Wiegeler, A., González, Y., and Sanromá, E.: Consistency and quality assessment of the Metop-A/IASI and Metop-B/IASI operational trace gas products (O<sub>3</sub>, CO, N<sub>2</sub>O, CH<sub>4</sub>, and CO<sub>2</sub>) in the subtropical North Atlantic, *Atmospheric Measurement Techniques*, 9, 2315–2333, doi:10.5194/amt-9-2315-2016, 2016.
- 10 Hase, F., Hanningan, J. W., Coffey, M. T., Goldman, A., Höfner, M., Jones, N. B., Rinsland, C. P., and Wood, S. W.: Intercomparison of retrieval codes used for the analysis of high-resolution ground-based FTIR measurements, *Journal of Quantitative Spectroscopy and Radiative Transfer*, 87, 25–52, 2004.
- Huang, J., Golombek, A., Prinn, R., Weiss, R., Fraser, P., Simmonds, P., Dlugokencky, E., Hall, B., Elkins, J., Steele, P., Langenfelds, R., Krummel, P., Dutton, G., and Porter, L.: Estimation of regional emissions of nitrous oxide from 1997 to 2005 using multinetwork  
15 measurements, a chemical transport model, and an inverse method, *Journal of Geophysical Research*, 113, doi:doi:10.1029/2007JD009381, 2008.
- Jones, A., Walker, K. A., Jin, J. J., Taylor, J. R., Boone, C. D., Bernath, P. F., Brohede, S., Manney, G. L., McLeod, S., Hughes, R., and Daffer, W. H.: Technical Note: A trace gas climatology derived from the Atmospheric Chemistry Experiment Fourier Transform Spectrometer (ACE-FTS) data set, *Atmospheric Chemistry and Physics*, 12, 5207–5220, doi:10.5194/acp-12-5207-2012, 2012.
- 20 Kort, E. A., Patra, P. K., Ishijima, K., Daube, B. C., Jimenez, R., Elkins, J., Hurst, D., Moore, F. L., Sweeney, C., and Wofsy, S. C.: Tropospheric distribution and variability of N<sub>2</sub>O: Evidence for strong tropical emissions, *Geophysical Research Letters*, 38, doi:doi:10.1029/2011GL047612, 2011.
- Masiello, G., Liuzzi, G., Serio, C., and Venafra, S.: Using the full IASI spectrum for the physical retrieval of Temperature, Water Vapour, Ozone and minor and trace gases: CO, CO<sub>2</sub>, CH<sub>4</sub>, N<sub>2</sub>O, SO<sub>2</sub>, HNO<sub>3</sub> and NH<sub>3</sub>, IASI Conference 2016, Antibes Juan-les-Pins, France,  
25 2016.
- Masuda, K., Takashima, T., and Takayama, Y.: Emissivity of pure and sea waters for the model sea surface in the infrared window regions, *Remote Sensing Environment*, 24, 313–329, doi:doi:10.1016/0034-4257(88)90032-6, 1988.
- Payan, S., Camy-Peyret, C., Oelhaf, H., Wetzell, G., Maucher, G., Keim, C., Pirre, M., Huret, N., Engel, A., Volk, M. C., Kuellmann, H., Kuttippurath, J., Cortesi, U., Bianchini, G., Mencaraglia, F., Raspollini, P., Redaelli, G., Vigouroux, C., De Mazière, M., Mikuteit, S.,  
30 Blumenstock, T., Velasco, V., Notholt, J., Mahieu, E., Duchatelet, P., Smale, D., Wood, S., Jones, N., Piccolo, C., Payne, V., Bracher, A., Glatthor, N., Stiller, G., Grunow, K., Jeseck, P., Te, Y., and Butz, A.: Validation of version-4.61 methane and nitrous oxide observed by MIPAS, *Atmospheric Chemistry and Physics*, 9, 413–442, doi:10.5194/acp-9-413-2009, 2009.
- Plieninger, J., von Clarmann, T., Stiller, G. P., Grabowski, U., Glatthor, N., Kellmann, S., Linden, A., Haenel, F., Kiefer, M., Höpfner, M., Laeng, A., and Lossow, S.: Methane and nitrous oxide retrievals from MIPAS-ENVISAT, *Atmospheric Measurement Techniques*, 8,  
35 4657–4670, doi:10.5194/amt-8-4657-2015, <http://www.atmos-meas-tech.net/8/4657/2015/>, 2015.
- Razavi, A., Clerbaux, C., Wespes, C., Clarisse, L., Hurtmans, D., Payan, S., Camy-Peyret, C., and Coheur, P. F.: Characterization of methane retrievals from the IASI space-borne sounder, *Atmospheric Chemistry and Physics*, 9, 7889–7899, doi:10.5194/acp-9-7889-2009, 2009.



- Risi, C., Noone, D., Worden, J., Frankenberg, C., Stiller, G., Kiefer, M., Funke, B., Walker, K., Bernath, P., Schneider, M., Wunch, D., Sherlock, V., Deutscher, N., Griffith, D., Wennberg, P., Strong, K., Barthlott, S., Hase, F., Garcia, O., Smale, D., Mahieu, E., Sayres, D., Bony, S., Lee, J., Brown, D., Uemura, R., , and Sturm, C.: Process-evaluation of tropospheric humidity simulated by general circulation models using water vapor isotopic observations. Part 1: comparison between models and datasets, *Journal Geophysics Research*, 117, doi:doi:10.1029/2011JD016621, 2012.
- 5 Rodgers, C.: *Inverse Methods for Atmospheric Sounding: Theory and Praxis*, World Scientific Publishing Co., Singapore, 2000.
- Rothman, L. S., Gordon, I. E., Barbe, A., Benner, D. C., Bernath, P. F., Birk, M., Boudon, V., Brown, L. R., Campargue, A., Champion, J.-P., Chance, K., Coudert, L. H., Dana, V., Devi, V. M., Fally, S., Flaud, J.-M., Gamache, R. R., Goldman, A., Jacquemart, D., Kleiner, I., Lacombe, N., Lafferty, W., Mandin, J.-Y., Massie, S. T., Mikhailenko, S. N., Miller, C. E., Moazzen-Ahmadi, N., Naumenko, O. V., Nikitin, A. V., Orphal, J., Perevalov, V. I., A. Perrin, A. P.-C., Rinsland, C. P., Rotger, M., Šimečková, M., Smith, M. A. H., Sung, K., Tashkun, S. A., Tennyson, J., Toth, R. A., Vandaele, A. C., and VanderAuwera, J.: The HITRAN 2008 Molecular Spectroscopic Database, *J. Quant. Spectrosc. and Rad. Transfer*, 110, 533–572, 2009.
- 10 Rothman, L. S., Gordon, I. E., Babikov, Y., Barbe, A., Benner, D. C., Bernath, P., Birk, M., Bizzocchi, L., Boudon, V., Brown, L., Campargue, A., Chance, K., Cohen, E., Coudert, L., Devi, V., Drouin, B., Fayt, A., Flaud, J.-M., Gamache, R., Harrison, J., Hartmann, J.-M., Hill, C., Hodges, J., Jacquemart, D., Jolly, A., Lamouroux, J., Roy, R. L., Li, G., Long, D., Lyulin, O., Mackie, C., Massie, S., Mikhailenko, S., Muller, H., Naumenko, O., Nikitin, A., Orphal, J., Perevalov, V., Perrin, A., Polovtseva, E., Richard, C., Smith, M., Starikova, E., Sung, K., Tashkun, S., Tennyson, J., Toon, G., Tyuterev, V., and Wagner, G.: The HITRAN 2012 Molecular Spectroscopic Database, *J. Quant. Spectrosc. and Rad. Transfer*, 130, 4–50, 2013.
- 15 Santoni, G. W., Daube, B. C., Kort, E. A., Jiménez, R., Park, S., Pittman, J. V., Gottlieb, E., Xiang, B., Zahniser, M. S., Nelson, D. D., McManus, J. B., Peischl, J., Ryerson, T. B., Holloway, J. S., Andrews, A. E., Sweeney, C., Hall, B., Hintsa, E. J., Moore, F. L., Elkins, J. W., Hurst, D. F., Stephens, B. B., Bent, J., and Wofsy, S. C.: Evaluation of the airborne quantum cascade laser spectrometer (QCLS) measurements of the carbon and greenhouse gas suite - CO<sub>2</sub>, CH<sub>4</sub>, N<sub>2</sub>O, and CO - during the CalNex and HIPPO campaigns, *Atmospheric Measurement Techniques*, 7, 1509–1526, doi:10.5194/amt-7-1509-2014, 2014.
- 20 Schneider, M. and Hase, F.: Optimal estimation of tropospheric H<sub>2</sub>O and δD with IASI/METOP, *Atmospheric Chemistry and Physics*, 11, 11 207–11 220, doi:10.5194/acp-11-11207-2011, 2011.
- 25 Schneider, M., Blumenstock, T., Chipperfield, M., Hase, F., Kouker, W., Ruhnke, R., Cuevas, E., and Fisher, H.: Subtropical trace gas profiles determined by ground-based FTIR spectroscopy at Izaña (28°N, 16°W): Five-year record, error analysis, and comparison with 3-D CTMs, *Atmospheric Chemistry and Physics*, 5, 153–167, 2005.
- Schneider, M., Barthlott, S., Hase, F., González, Y., Yoshimura, K., García, O. E., Sepúlveda, E., Gomez-Pelaez, A., Gisi, M., Kohlhepp, R., Dohe, S., Blumenstock, T., Wiegeler, A., Christner, E., Strong, K., Weaver, D., Palm, M., Deutscher, N. M., Warneke, T., Notholt, J., Lejeune, B., Demoulin, P., Jones, N., Griffith, D. W. T., Smale, D., and Robinson, J.: Ground-based remote sensing of tropospheric water vapour isotopologues within the project MUSICA, *Atmospheric Measurement Techniques*, 5, 3007–3027, doi:10.5194/amt-5-3007-2012, 2012.
- 30 Schneider, M., González, Y., Dyroff, C., Christner, E., Wiegeler, A., Barthlott, S., García, O. E., Sepúlveda, E., Hase, F., Andrey, J., Blumenstock, T., Guirado, C., Ramos, R., and Rodríguez, S.: Empirical validation and proof of added value of MUSICA's tropospheric δD remote sensing products, *Atmospheric Measurement Techniques*, 8, 483–503, doi:10.5194/amt-8-483-2015, 2015.
- Schneider, M., Wiegeler, A., Barthlott, S., González, Y., Christner, E., Dyroff, C., García, O. E., Hase, F., Blumenstock, T., Sepúlveda, E., Mengistu Tsidu, G., Takele Kenea, S., Rodríguez, S., and Andrey, J.: Accomplishments of the MUSICA project to provide accurate,



- long-term, global and high-resolution observations of tropospheric  $\{H_2O, \delta D\}$  pairs – a review, *Atmospheric Measurement Techniques*, 9, 2845–2875, doi:10.5194/amt-9-2845-2016, 2016.
- Seemann, S., Borbas, E., Knuteson, R., Stephenson, G., and Huang, H.-L.: Development of a Global Infrared Land Surface Emissivity Database for Application to Clear Sky Sounding Retrievals from Multispectral Satellite Radiance Measurements, *Journal of Applied Meteorology and Climatology*, 47, 108–123, doi:DOI: 10.1175/2007JAMC1590.1, 2008.
- 5 Sepúlveda, E., Schneider, M., Hase, F., Barthlott, S., Dubravica, D., García, O. E., Gómez-Peláez, A., González, Y., Guerra, J. C., Gisi, M., Kohlhepp, R., Dohe, S., Blumenstock, T., Strong, K., Weaver, D., Palm, M., Sadeghi, A., Deutscher, N. M., Warneke, T., Notholt, J., Jones, N., Griffith, D. W. T., Smale, D., Brailsford, G. W., Robinson, J., Meinhardt, F., Steinbacher, M., Aalto, T., and Worthy, D.: Tropospheric  $CH_4$  signals as observed by NDACC FTIR at globally distributed sites and comparison to GAW surface in situ measurements, *Atmospheric Measurement Techniques*, 7, 2337–2360, doi:10.5194/amt-7-2337-2014, 2014.
- 10 Stocker, T. F., Qin, D., Plattner, G.-K., Tignor, M., Allen, S. K., Boschung, J., Nauels, A., Xia, Y., Bex, V., and Midgley, P. M.: *Climate Change 2013: The Physical Science Basis*, Tech. rep., 1535 pp., 2013.
- Tikhonov, A.: On the solution of incorrectly stated problems and a method of regularization, *Dokl. Acad. Nauk SSSR*, 151, 501–504, 1963.
- Wecht, K. J., Jacob, D. J., Wofsy, S. C., Kort, E. A., Worden, J. R., Kulawik, S. S., Henze, D. K., Kopacz, M., and Payne, V. H.: Validation of TES methane with HIPPO aircraft observations: implications for inverse modeling of methane sources, *Atmospheric Chemistry and Physics*, 12, 1823–1832, doi:10.5194/acp-12-1823-2012, 2012.
- 15 Wiegele, A., Schneider, M., Hase, F., Barthlott, S., García, O. E., Sepúlveda, E., González, Y., Blumenstock, T., Raffalski, U., Gisi, M., and Kohlhepp, R.: The MUSICA MetOp/IASI  $H_2O$  and  $\delta D$  products: characterisation and long-term comparison to NDACC/FTIR data, *Atmospheric Measurement Techniques*, 7, 2719–2732, doi:10.5194/amt-7-2719-2014, 2014.
- Wofsy, S. C., the HIPPO Science Team, Modellers, C., and Teams, S.: HIAPER Pole-to-Pole Observations (HIPPO): fine-grained, global-scale measurements of climatically important atmospheric gases and aerosols, *Philosophical Transactions of the Royal Society A*, 369, 2073–2086, 2011.
- 20 Worden, J., Kulawik, S., Frankenberg, C., Payne, V., Bowman, K., Cady-Peirara, K., Wecht, K., Lee, J.-E., and Noone, D.: Profiles of  $CH_4$ , HDO,  $H_2O$ , and  $N_2O$  with improved lower tropospheric vertical resolution from Aura TES radiances, *Atmospheric Measurement Techniques*, 5, 397–411, doi:10.5194/amt-5-397-2012, 2012.
- 25 Wunch, D., Toon, G. C., Blavier, J.-F. L., Washenfelder, R. A., Notholt, J., Connor, B. J., Griffith, D. W. T., Sherlock, V., and Wennberg, P. O.: The total carbon column observing network, *Philosophical Transactions of the Royal Society - Series A: Mathematical, Physical and Engineering Sciences*, doi:doi:10.1098/rsta.2010.0240, 2011.
- Xiong, X., Barnet, C., Maddy, E. S., Gambacorta, A., King, T. S., and Wofsy, S. C.: Mid-upper tropospheric methane retrieval from IASI and its validation, *Atmospheric Measurement Techniques*, 6, 2255–2265, doi:10.5194/amt-6-2255-2013, 2013.
- 30 Yokota, T., Yoshida, Y., Eguchi, N., Ota, Y., Tanaka, T., Watanabe, H., and Maksyutov, S.: Global Concentrations of  $CO_2$  and  $CH_4$  Retrieved from GOSAT: First Preliminary Results, SOLA, doi:doi:10.2151/sola.2009-041, 2009.

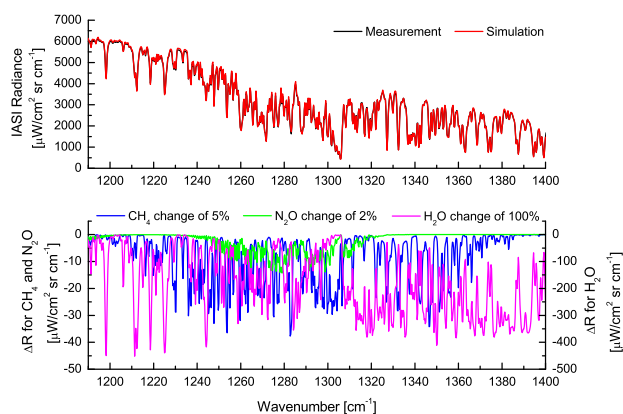


**Figure 1.** Top: example of spectral radiances recorded by IASI and the corresponding PROFFIT-nadir simulation over a tropical ocean pixel ( $\approx 12^\circ\text{S}$ ) in winter. Bottom: spectral changes of the IASI radiance ( $\Delta R$ ) due to a change of  $\text{CH}_4$  of 5%, of  $\text{N}_2\text{O}$  of 2% and of  $\text{H}_2\text{O}$  of 100% (please note the different y-axis scale for  $\text{H}_2\text{O}$ ).

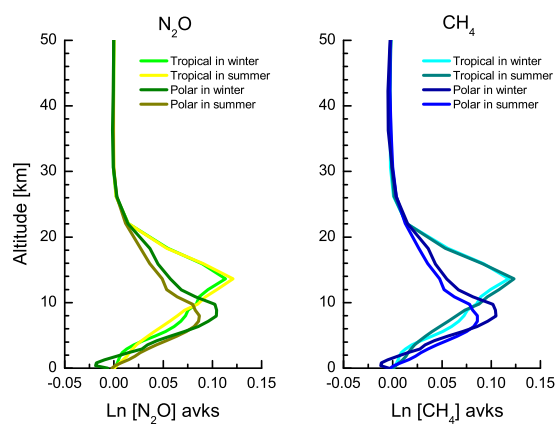


**Figure 2.** Example of row averaging kernels (avks) for  $\text{N}_2\text{O}$  (left panel) and  $\text{CH}_4$  (right panel) on logarithm scale in the high northern hemisphere ( $\approx 75^\circ\text{N}$ ) and the tropics ( $\approx 12^\circ\text{S}$ ) over ocean pixels in winter and in summer. The coloured lines represent the row kernels at the IASI maximum sensitivity: 8 km and 14 km for polar and tropics, respectively.

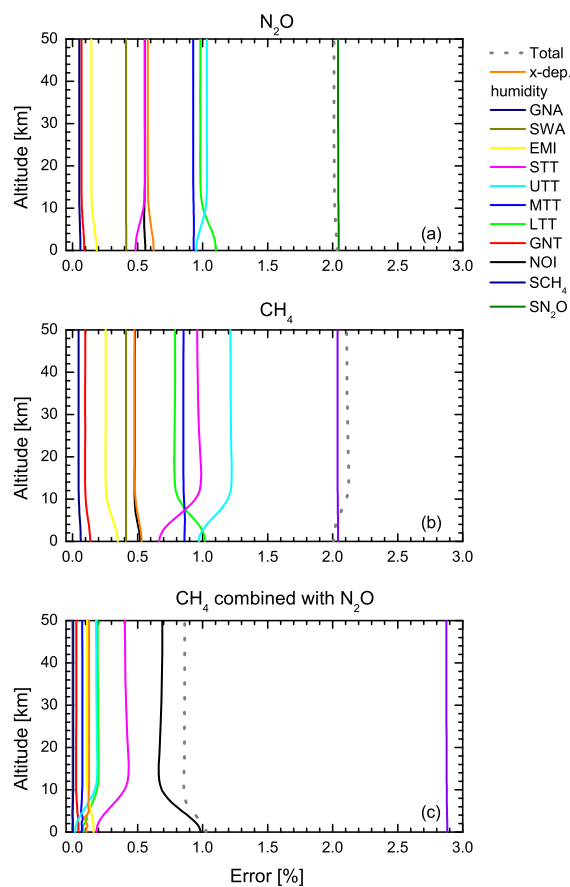


**Figure 3.** Top panel:  $\text{N}_2\text{O}$  error patterns over a mid-latitude pixel in summer ( $\approx 45^\circ\text{N}$ ), given by the square root of the diagonal of the error covariance matrix ( $S_\epsilon$ , Eq. 2) for all the uncertainties sources as listed in Table 1. "Total" means the root-squares-sum of the measurement noise and all the parameter errors, except for the spectroscopy ("SCH<sub>4</sub>" and "SN<sub>2</sub>O"). "x-dep. humidity" means the cross-dependence on humidity. Middle and bottom panels: same as top, but for CH<sub>4</sub> and CH<sub>4</sub> combined with the co-retrieved  $\text{N}_2\text{O}$  product.

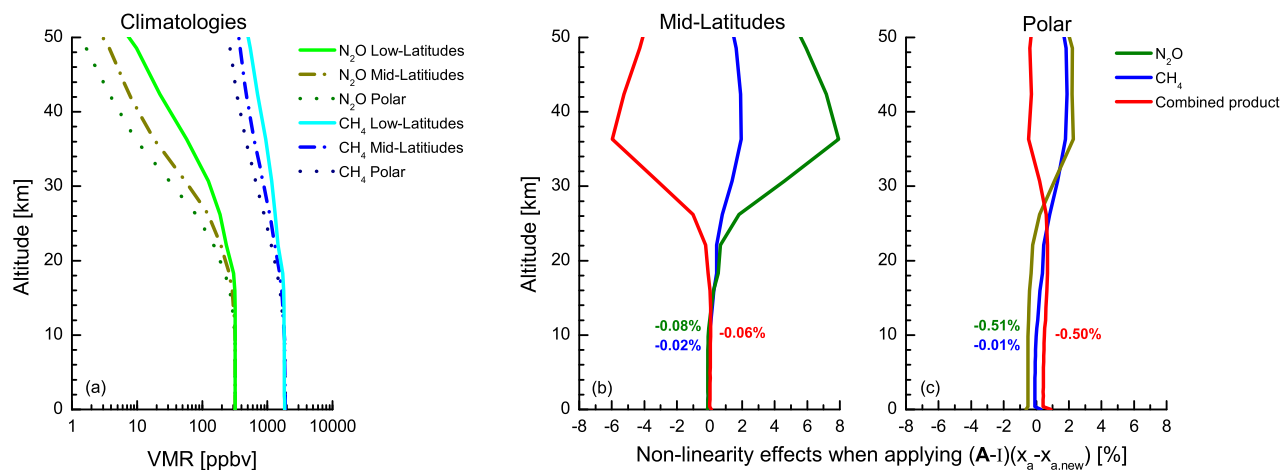


**Figure 4.** (a): Annual mean VMR averages over latitudinal bands (low-latitude, mid-latitude and polar regions) from WACCM-version 5 data for CH<sub>4</sub> and N<sub>2</sub>O. Note that the low-latitude climatological profile is the single a-priori we use for all the retrievals (for details see Sect. 2.2). (b) and (c): Typical non-linearity effects that have to be considered when changing the a-priori profiles by adding  $(\mathbf{A} - \mathbb{I})(\mathbf{x}_a - \mathbf{x}_{a,new})$  to the original retrieved states. Panel (b) for typical mid-latitude retrievals when changing the single low-latitude a-priori to a mid-latitude a-priori and (c) for typical polar retrievals when changing the single low-latitude a-priori to a polar a-priori. The non-linearity effect at the altitude of 10 km is written in the panels in their corresponding colours for CH<sub>4</sub>, N<sub>2</sub>O, and the combined product.

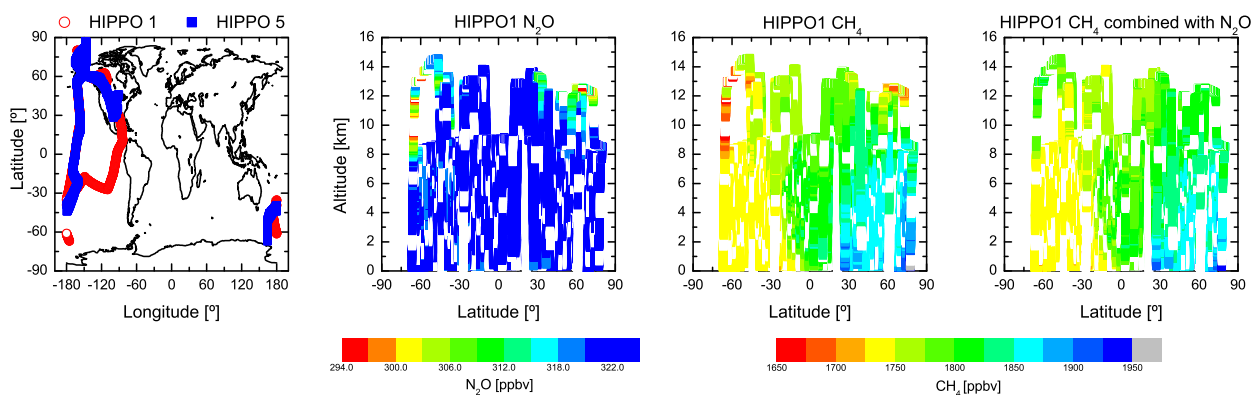


**Figure 5.** Overview of the HIPPO data used in this study. Left panel: geographical distribution of the aircraft profiles selected for validation: HIPPO1 in red and HIPPO5 in blue. Middle panels: latitudinal cross sections of N<sub>2</sub>O and CH<sub>4</sub> vertical profiles as measured during the HIPPO1 mission. Right panel: latitudinal cross section of vertical profiles of the combined product.

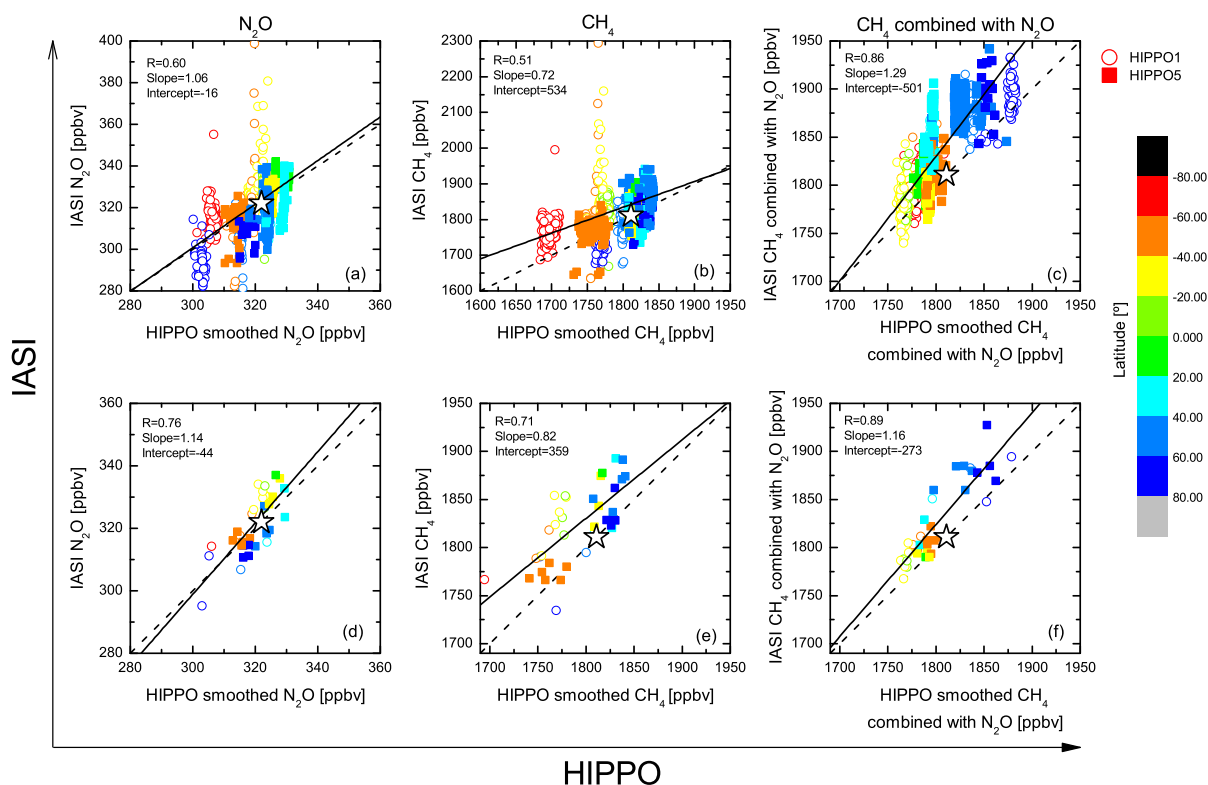


**Figure 6.** Correlation plots for the comparison between MUSICA/IASI and HIPPO data. Top panel: (a) scatter plot of the IASI  $\text{N}_2\text{O}$  VMR versus the HIPPO smoothed  $\text{N}_2\text{O}$  VMR at 10 km considering all IASI-HIPPO coincidences ( $N=1408$ ); (b) same as (a), but for  $\text{CH}_4$ ; (c) same as (a), but for the combined  $\text{CH}_4$  VMR with the simultaneous  $\text{N}_2\text{O}$  VMR observations. Bottom panel: same as top panel (d, e, and f), but averaging all the IASI observations within the collocation box of  $\pm 2^\circ$  latitude/longitude centred at each HIPPO mean location ( $N=36$ ). The stars indicate the a-priori VMR at 10 km used for the IASI retrievals, while the solid and dashed black lines represent the least squares fits and the diagonals ( $x=y$ ), respectively. The fit parameters are shown in the legend.

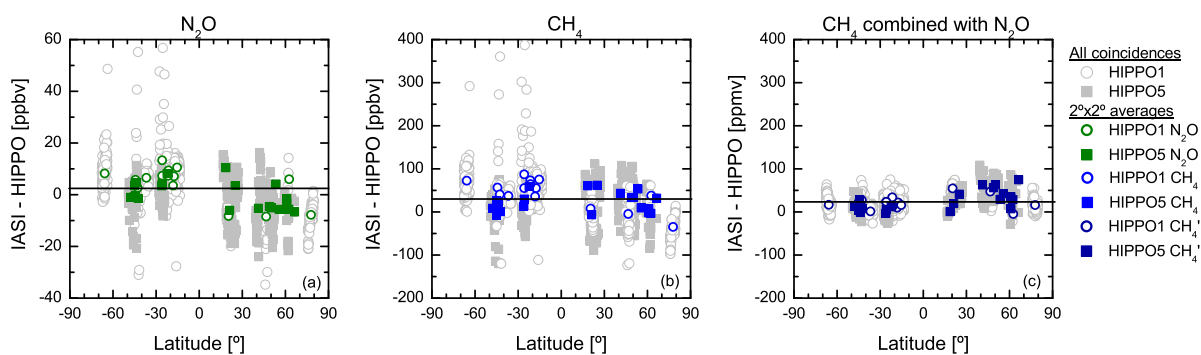


**Figure 7.** Difference between MUSICA/IASI and HIPPO products [in ppbv] versus latitude and HIPPO mission. (a)  $N_2O$ , (b)  $CH_4$ , and (c) combined product  $CH_4$ . The solid black lines represent the respective bias for the 2°x2° averages.

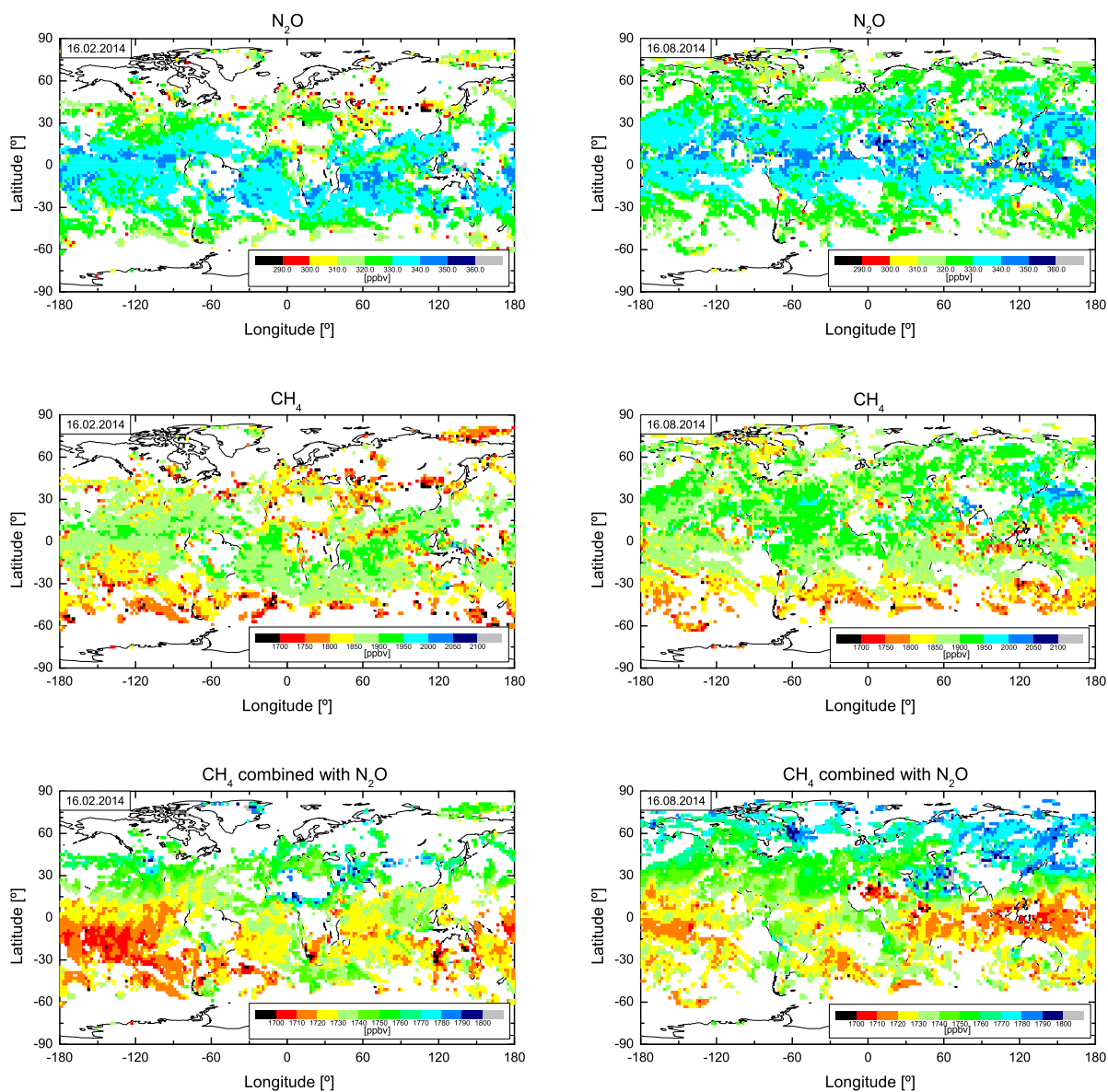


**Figure 8.** Upper panels: example of the MUSICA/IASI-A  $N_2O$  global maps at  $\approx 350$ -300 hPa in winter (16.02.2014, left panels) and in summer (16.08.2014, right panels). Middle and bottom panels: same as upper panels, but for  $CH_4$  and for the combined product, respectively.

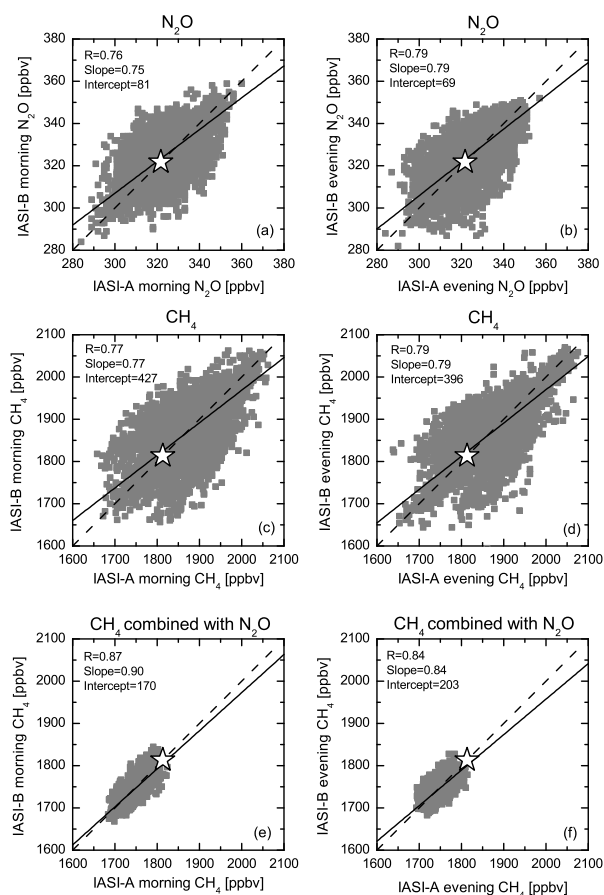


**Figure 9.** Example of IASI-A and IASI-B consistency assessment on 16.08.2014 for the IASI-A and IASI-B observations at a global scale being paired in  $0.25^\circ \times 0.25^\circ$  boxes. The stars indicate the a-priori used for the IASI retrievals, while the solid and dashed black lines represent the least squares fits and the diagonals ( $x=y$ ), respectively. The fit parameters are shown in the legend.

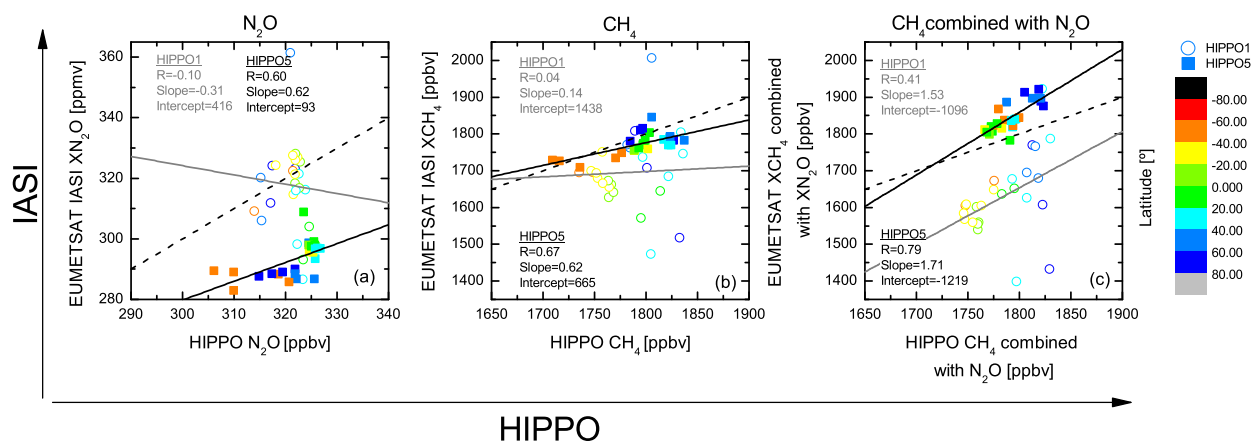


**Figure 10.** Same as Fig. 6, but for the EUMETSAT/IASI XCH<sub>4</sub> and XN<sub>2</sub>O products (2°x2° averages only) versus the HIPPO products at 10 km averaging all the IASI observations within the collocation box of ±2° latitude/longitude centred at each HIPPO mean location. The solid and dashed black lines represent the least squares fits and the diagonals (x=y), respectively. The fit parameters are shown in the legend.



**Table 1.** Uncertainty sources and values used for the CH<sub>4</sub> and N<sub>2</sub>O error estimation. "LTT", "MTT", "UTT", and "STT" represent the lower (0-2 km), middle (2-5 km), upper tropospheric (5-10 km), and the stratospheric temperature (above 10 km), while the spectroscopy parameters are the line strength (*S*), and the air pressure broadening coefficient ( $\gamma$ ).

Error source	Uncertainty
Measurement Noise (NOI)	$2 \times 10^{-2} \mu\text{W}/\text{cm}^2 \text{srcm}^{-1}$
Swath angle (SWA)	0.01 rad
Ground Temperature (GNT)	2 K
Atmospheric temperature (< 2 km) (LTT)	2 K
Atmospheric temperature (> 2 km) (MTT, UTT, and STT)	1 K
Emissivity (EMI)	1%
Ground altitude (GNA)	20 m
Spectroscopy for CH <sub>4</sub> and N <sub>2</sub> O ( <i>S</i> , and $\gamma$ )	2%, and 2%
Spectroscopy for H <sub>2</sub> O ( <i>S</i> , and $\gamma$ )	1%, and 5%
Cross-dependence on humidity	100% humidity variation



**Table 2.** Summary of statistics for MUSICA/IASI-HIPPO comparison. Bias, IP68, and STD corresponds to the median, the semi-distance between the percentiles 84.1<sup>th</sup> and 15.9<sup>th</sup>, and the standard deviation of the difference between IASI and HIPPO products (IASI-HIPPO). The statistical estimators are shown for the absolute differences [in ppbv] as well as for the relative differences with regard to the HIPPO values [in %]. R is the correlation coefficient, and CH<sub>4</sub> represents the combined product.

		All coincidences		2°x2° averages	
		[ppbv]	[%]	[ppbv]	[%]
N <sub>2</sub> O	Bias	2.8	0.9	3.4	1.1
	IP68	8.7	2.7	6.9	2.1
	STD	9.5	3.0	6.2	1.9
	R	0.60		0.76	
CH <sub>4</sub>	Bias	39.4	2.2	33.7	1.8
	IP68	38.2	2.1	32.1	1.7
	STD	47.2	2.7	28.9	1.6
	R	0.51		0.71	
CH <sub>4</sub> '	Bias	24.4	1.4	20.7	1.2
	IP68	26.3	1.5	21.8	1.2
	STD	24.7	1.4	20.3	1.1
	R	0.86		0.89	